Measuring the Neutrino Flux from the Galactic Plane with the PLEnuM Framework

Bachelor's Thesis in Physics

Presented by
Anke Mosbrugger
08.04.2024

Erlangen Centre for Astroparticle Physics
Friedrich-Alexander-Universität Erlangen-Nürnberg

Supervisor: Prof. Dr. Claudio Kopper

Abstract

Diffuse neutrino emission from the galactic plane has long been expected given the observed gamma ray flux. One of the recent successes of the IceCube neutrino observatory was the observation of high-energy neutrinos from the galactic plane. This observation will give further insight into cosmic ray propagation and galactic sources. However, due to its location at the geographic South Pole, IceCube's effective area in the direction of the galactic center region is limited. This limitation can be overcome by combining data from multiple neutrino telescopes with different fields of view, thereby increasing the analysis sensitivity. This concept is implemented in the Planetary Neutrino Monitoring System (PLEnuM). The PLEnuM software uses parametrized instrument response functions to facilitate the combination of datasets from multiple detectors.

Within this thesis, the galactic plane analysis is implemented in PLEnuM and applied to public IceCube data. The analysis uses a three-dimensional likelihood fit to distinguish a galactic component from atmospheric and diffuse astrophysical neutrinos. Due to limitations of the analysis, the result is not statistically significant. However, the best-fit galactic flux is consistent with previous IceCube results.

Contents

1 Introduction

The galactic plane has long been expected to emit diffuse neutrinos due to the observed gamma-ray flux. In 2023 the IceCube Collaboration published an article "Observation of high-energy neutrinos from the galactic plane" [5]. Within this work, an only isotropic background is rejected with $4.5\,\sigma$ significance. Concluding there must be a diffuse galactic neutrino flux [5]. This observation will provide insight into cosmic ray propagation and galactic neutrino sources.

The IceCube neutrino telescope is located at the geographic South Pole. So IceCube's effective area is limited in the southern sky, where the galactic center is located. To overcome the limitations, multiple neutrino telescopes on Earth with different fields of view can be combined. This concept is introduced by the Planetary Neutrino Monitoring System (PLEnuM). Combining the data from different neutrino telescopes, results in an increased sensitivity of the analysis. IceCube-sized telescopes such as KM3NeT, P-ONE, and Baikal-GVD, including IceCube itself, are combined in PLEnuM-1. Adding additional future detectors (PLEnuM-2) to the analysis e.g. IceCube-Gen2, will increase the sensitivity even further [15].

In this thesis, the analysis of the galactic plane is implemented in the PLEnuM framework. This is achieved by using models for all neutrino flux components that are detected: atmospheric background, isotropic astrophysical flux, and galactic neutrino flux. Furthermore, the contribution or the galactic flux model, called CRINGE, is tested using public IceCube data. The flux models are fitted to these data using a three-dimensional binned maximum likelihood method. Additionally, to determine the significance of the galactic contribution in the dataset, a hypothesis test is performed.

The analysis of the galactic plane performed in this thesis is evaluated by comparing it with the analysis performed by Philip Fürst on behalf of the IceCube collaboration [8]. Both analyses include the same neutrino flux models but use different IceCube datasets.

2 Neutrinos

Neutrinos and their anti-particles, the anti-neutrinos, are electrically neutral leptons. There are three neutrino flavors: electron-neutrino ν_e, muon-neutrino ν_μ and tau-neutrino ν_τ. Neutrinos only interact with matter by weak interaction processes. Due to their low cross section with matter, they are ideal messenger particles for astronomy. Neutrinos from astrophysical sources can propagate unhindered over great distances. By using neutrino telescopes on Earth, it is possible to reconstruct their path to identify their origin [9].

Neutrinos originate from different sources. In this thesis, only high-energetic neutrinos are considered. These are created by cosmic rays in the atmosphere or in astrophysical neutrino sources, including the Milky Way or extra-galactic sources [5]. These neutrino sources contribute to a total high-energy neutrino flux which can be measured at the Earth. The components of this flux are discussed in the following section.

2.1 Atmospheric Neutrino Background Flux

The dominating part of the total high-energy neutrino flux measured at Earth is the atmospheric background. It is created by high-energy cosmic rays, mainly consisting of protons, arriving approximately isotropic at the Earth's atmosphere. Interaction processes in the Earth's atmosphere result in hadronic showers. The dominant production channel for neutrinos is via pion $\pi^\pm$ and kaon $K^\pm$ decay [9]. These mesons decay quickly into atmospheric muons and atmospheric neutrinos[9]:

$$\pi^\pm \to \mu^\pm + \overset{(-)}{\nu}_\mu$$
$$K^\pm \to \mu^\pm + \overset{(-)}{\nu}_\mu.$$

Higher energy muons can reach the Earth's surface and can be detected there. Muons with an energy below a few GeV decay before reaching the Earth´s surface. In the muon decay an anti-electron-neutrino and a muon-neutrino are produced [9]:

$$\mu^\pm \to e^\pm + \overset{(-)}{\nu}_e + \overset{(-)}{\nu}_\mu.$$

The background neutrino flux does not have a uniform angular distribution in declination at the Earth´s surface. Muons coming from the horizon have a longer distance to travel, thus a higher probability of decay. So a higher atmospheric neutrino background is measured for small declination angles δ. In right ascension α, one assumes a uniform angular distribution except for neutrinos below 400 MeV where geomagnetic effects are dominant [13]. This effect is negligible in the following analysis, as only neutrino events above 10^2 GeV are considered.

2.2 Astrophysical Neutrino Flux

In 2013 the IceCube Collaboration found evidence for a diffuse neutrino flux, which is isotropically distributed and of astrophysical origin. By investigating the total neutrino flux and its properties one gains insights into the acceleration and propagation of high-energy cosmic rays and the corresponding neutrino sources [1].

Potential sources for high-energy neutrinos are active galactic nuclei (AGNs), tidal disruption events (TDEs), or chocked gamma-ray bursts (GRBs) in dense environments [1]. All these sources have in common that cosmic rays, following a power law in energy distribution, interact with gas or photon fields in or near the source. In the interaction process, kaons and pions are produced which decay into neutrinos. The energy of these neutrinos follows the same power-law behavior as the cosmic rays starting the neutrino production [1].

In particular the IceCube analysis "Improved Characterization of the Astrophysical Muon–neutrino Flux with 9.5 Years of IceCube Data", 2022, reports a diffuse astrophysical flux, excluding a purely atmospheric neutrino flux with $5.6\,\sigma$. The data used in this analysis are consistent with an energy spectrum modeled by a single power-law. The single power law is characterized by a normalization parameter $\Phi^{\nu_\mu+\bar{\nu}_\mu}_{@100\mathrm{TeV}} = 1.44^{+0.25}_{-0.26}$ (this parameter is provided without a specified unit, cf. Equation 4.1) and the spectral index $\gamma_{\mathrm{SPL}} = 2.37^{+0.09}_{-0.09}$ [1].

2.3 Galactic Neutrino Flux

In 2023 the IceCube Collaboration published the article "Observation of high-energy neutrinos from the galactic plane". In this work, the neutrino emission from the galactic plane is identified as a non-isotropic part of the astrophysical neutrino flux, rejecting only isotropic background with $4.5\,\sigma$ [5].

The search for the galactic contribution of astrophysical neutrinos was motivated by knowing the gamma-ray flux from the galactic plane. In gamma rays with energies above 1 GeV the Milky Way is the most prominent feature. The galactic plane band in galactic coordinates is shown in Figure 2.1. Most of the gamma rays are produced by the decay of a neutral pion π^0 which is produced by cosmic rays interacting with the interstellar medium of the Milky Way [5].

In the interaction process with cosmic rays and the interstellar medium, also charged pions $\pi^\pm$ are produced. The pions decay and produce neutrinos. In comparison to photons, neutrinos have a low cross-section for interactions with matter. Thus they mostly do not interact with matter during their path to the Earth. Therefore, if the arrival direction of a neutrino is known, it is possible to reconstruct the location of its origin [5].

As the production of photons and neutrinos by the same process is present in the Milky Way and a high gamma-ray flux is observed, a diffuse galactic neutrino flux is expected (cf. Figure 2.1). The diffuse galactic neutrino is modeled using the Fermi-π^0 model. However, in this thesis, the CRINGE model is utilized to describe the diffuse galactic neutrino flux. The details of the CRINGE model, which is used for flux modeling, can be found in subsection 4.3.

Additionally, the Milky Way has several gamma-ray point sources which are potential cosmic-ray accelerators. Therefore, a higher galactic neutrino flux than only the diffuse galactic flux is expected [5].

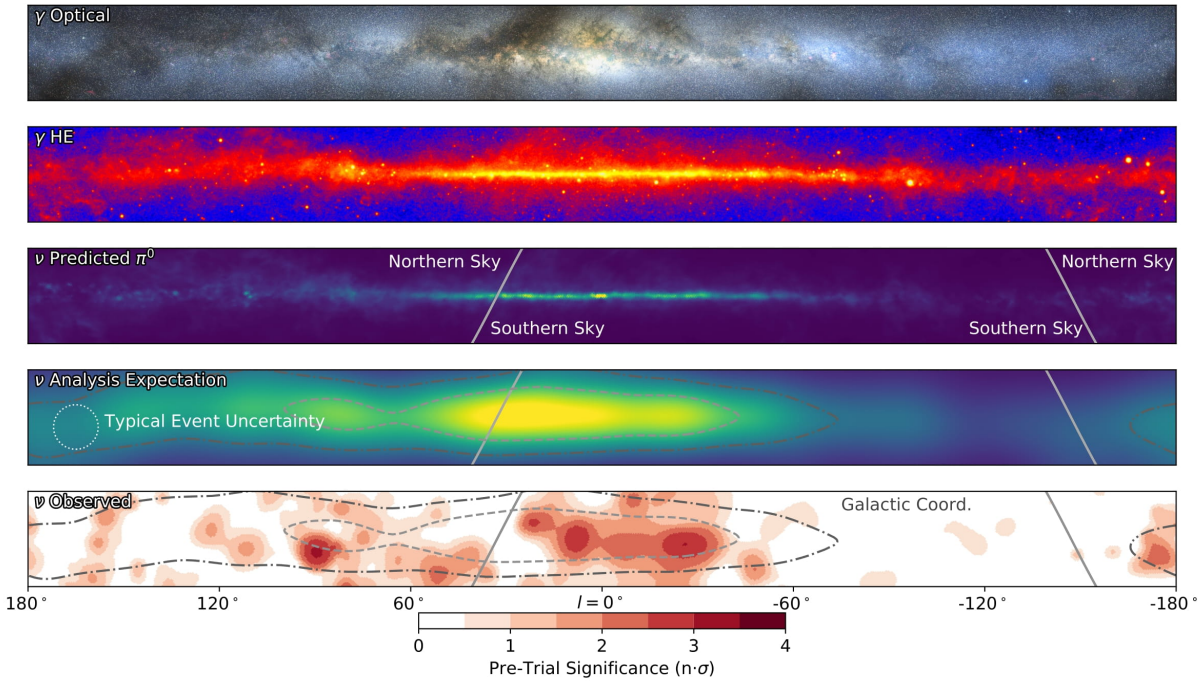

Figure 2.1: The galactic plane visualized for different messengers. All messengers are shown in galactic coordinates in a band of ±15°. From top to bottom the messengers shown are: 1) the optical photon range 2) the integrated gamma-ray flux observed by the Fermi-LAT survey 3) the expected neutrino flux by considering the Fermi-LAT survey 4) the expected neutrino flux seen by IceCube for cascade-like neutrino events 5) significance of observed neutrinos in the galactic plane band in the all-sky scan for point-like sources using cascade neutrino events of the IceCube collaboration [5]. Image taken from the IceCube Collaboration.

3 IceCube

Within this thesis, public IceCube data is used. The IceCube neutrino telescope is located at the geographic South Pole and is designed to measure high-energy astrophysical neutrinos. These are neutrinos in the energy range between 100 GeV - 10 PeV. IceCube consists of 5,160 digital optical modules (DOMs) attached to 86 strings. Each string was lowered into boreholes in the ice. The DOMs are situated at a depth of 1.45 km to 2.45 km below the ice surface and distributed over a volume of 1 km^3 (cf. Figure 3.1). Such large-volume neutrino detectors are necessary because of the low cross-section for neutrino-matter interactions. The IceTop unit on the ice surface is used to measure air showers from primary cosmic rays [4].

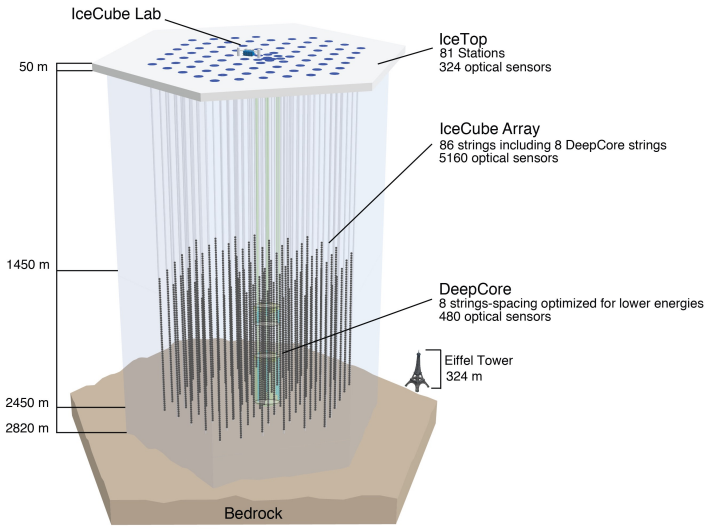

Figure 3.1: Sketch of IceCube's structure consisting of 86 strings with 5,160 DOMs distributed over 1 km^3 in the Antarctic ice. On the ice surface, IceTop is located. Image taken from the IceCube Collaboration.

3.1 Event Signatures

Neutrinos interact only through weak interaction. This is the reason why it is difficult to measure them directly. However, if a neutrino interacts via charged-current (CC) or neutral-current (NC) interaction with matter, charged secondary particles are produced. As these charged particles travel through the ice faster than the speed of light in ice, Cherenkov light is emitted. Due to the Antarctic ice being transparent, the Cherenkov light is detected by PMTs (Photo Multiplier Tubes) in the DOMs and the neutrino are indirectly observed [4].

Cherenkov neutrino telescopes have two main event signatures for different interactions in the detector: Cascades and tracks. For high-energy neutrinos ($E_\nu > 100\,\mathrm{GeV}$) the dominant interaction between neutrinos and nucleons of the target material, here ice, is deep-inelastic scattering. Therefore cascade-like events originate from a NC interaction with the nucleon N and all flavor neutrinos ν_l: $\nu_l + N \rightarrow \nu_l + X$. This interaction is mediated by a Z^0-boson and the neutrino leaving the interaction vertex has a reduced energy. Additionally, a hadron shower X is produced

which interacts directly with the medium around the point of interaction and is responsible for the cascade structure of that event. Cascade-like events also result from a CC interaction of nucleons and electron neutrinos ν_e: $\nu_e + N \rightarrow e^- + X$, which is mediated by a W^--boson. The produced electron and hadrons also interact with the medium near the interaction point [9, 18].

The more important event signature for this thesis is track-like events that result from the CC interaction of nucleons and muon neutrinos ν_μ:

$$\nu_\mu + N \rightarrow \mu^- + X.$$

Additionally to the hadron cascade, a high-energetic muon is created. Muons with high energies can travel for several kilometers through the ice. On their path through the detector, they create a track-like signature while losing energy. Even muon neutrino CC interactions happening outside of the detector can be reconstructed by detecting the outgoing muon. Therefore the effective volume of a Cherenkov neutrino telescope can be larger than the actual detector size [18].

One major problem for detecting track-like neutrino events is that these are not distinguishable from high-energy muons created from cosmic rays in the atmosphere. IceCube is located deep in the ice to shield the detector from atmospheric muons. This is only feasible for lower energetic muons and high-energetic muons reach the detector nonetheless [18].

For this reason, it is advantageous to use only upgoing muon tracks in the neutrino telescope to create a pure data set. Up-going means that only muons coming from the direction of the Earth, for IceCube the northern hemisphere, are considered. So the IceCube data are cut at a declination angle of $\delta = -5°$. As atmospheric muons are created in the atmosphere and are so short-lived that they decay or are absorbed before crossing the Earth, muons coming out of the Earth must be created by CC neutrino interactions in the surrounding medium.

As mentioned in subsection 2.3 the galactic center is located in the southern sky. Therefore it can not be observed by up-going track-like events in IceCube. Only a part of the Milky Way as seen in Figure 4.3 can be observed with such an data set in IceCube.

3.2 Effective Area

As mentioned in subsection 3.1, the detection volume of IceCube is larger than its actual size for track-like events. According to the definition, the effective area is "the size of the hypothetical area A_{eff} on which 100% of neutrinos would be detected when crossing this area" [2]. This area is strongly energy dependant [6].

When analyzing only up-going neutrinos, the Earth's absorption must be taken into account for determining the effective area. The expected neutrino flux depends on the incoming neutrino's declination. Neutrinos with a declination of less than $\delta < 30°$ have to cross less matter in the Earth than those with a larger declination angle. The Earth's absorption is energy dependent. The Earth becomes opaque for neutrinos with energies above 0.1 PeV, as neutrinos with higher energy have a higher cross-section. In contrast to that, for neutrinos with lower energy, the Earth becomes less opaque. In consequence, the effective area of Ice Cube is strongly dependent on the muon track's declination and the muon neutrino energy [15, 18].

IceCube is located at the geographical South Pole and the Earth rotates around the axis, which is built up by the geographical North and South Poles. Therefore it is assumed that IceCube´s effective area is constant in right ascension when considering timescales >> 1 day.

The effective area of the IceCube detector is determined by Monte Carlo simulations. The result is an effective area A_{eff} depending on the neutrino Energy E_ν, declination δ, and is constant in right ascension α. The simulated effective area already implemented in PLEnuM depending on energy and right ascension is shown in Figure 3.2.

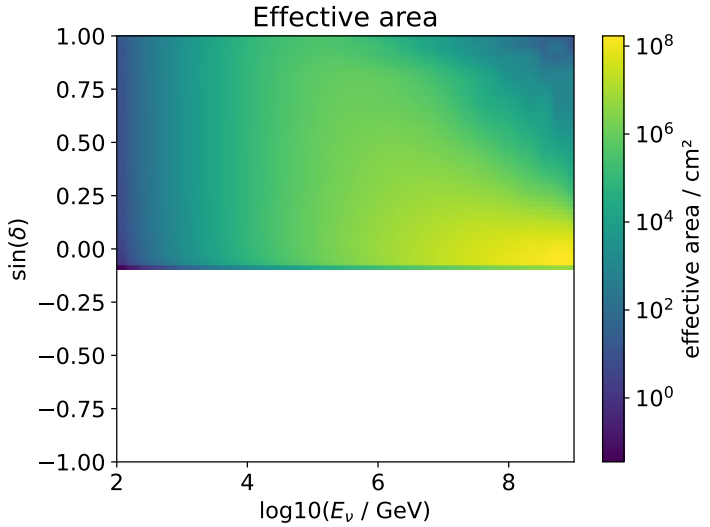

Figure 3.2: Simulated effective area implemented in PLEnuM which is cut at $\delta = -5°$.

4 Neutrino Flux Models

The significance of a galactic neutrino flux contribution to the total high-energy neutrino flux is tested in this thesis. To perform such a study precise models of each contribution to the total neutrino flux are necessary. In the following analysis, model parameters are extracted from the observed neutrino events in IceCube.

4.1 Atmospheric Background Flux Model

The atmospheric background is modeled by the Matrix Cascade Equations (MCEq) code. It models the atmospheric neutrino flux by solving cascade equations for particle cascades in the atmosphere including particle production, decay, and interaction [12]. This flux model was already implemented in PLEnuM in dependance of the energy E_ν and the declination angle δ of the simulated neutrinos as shown in Figure 4.1.

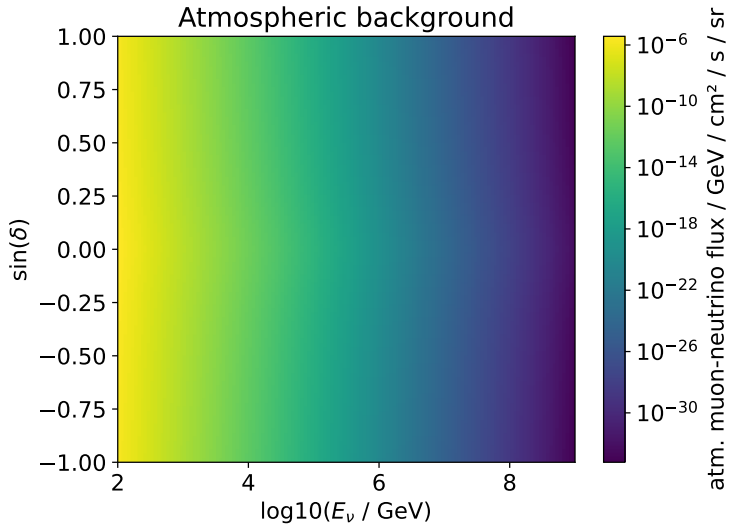

Figure 4.1: Atmospheric background flux model implemented in PLEnuM depending on energy and declination. The flux is given in units of atm. background flux / GeV / cm^2 / s / sr.

The simulated background flux is normalized by the parameter $\Phi_{\text{background}}$. This model parameter is determined by detector data.

4.2 Diffuse Flux Model

Another contribution to the total neutrino flux comes from diffuse astrophysical neutrinos. These are isotropically distributed and roughly follow a power law as mentioned in section 2.

Thus the all-flavor diffuse astrophysical flux $\frac{\mathrm{d}\Phi_\nu}{\mathrm{d}E_{\nu\,\text{diffuse}}}$ is modeled by postulating a power law [14]:

$$\frac{\mathrm{d}\Phi_\nu}{\mathrm{d}E_{\nu\,\text{diffuse}}} = \Phi_{\text{diffuse}}(E_\nu \,/\, 10^5\,\mathrm{GeV})^{-\gamma_{\text{astro}}}\, 10^{-18}\,\mathrm{GeV}^{-1}\,\mathrm{cm}^{-2}\,\mathrm{s}^{-1}\,\mathrm{sr}^{-1} \tag{4.1}$$

In this equation, E_ν is the neutrino energy, Φ_{diffuse} is the normalization parameter, and γ_{astro} is the spectral index. The normalization parameter and the spectral index are free parameters that are determined from data. This model was already implemented in PLEnuM with energy and declination dependence.

4.3 CRINGE Flux Model

A precise model for the galactic plane is needed to test the contribution of galactic neutrinos in the measured neutrino data. As no analysis of the galactic plane had been done before in PLEnuM, the CRINGE (Cosmic Ray-fitted Intensities of Galactic Emission) model was implemented as part of this thesis to model the neutrino flux in the galactic plane. For this model, only a normalization parameter Φ_{cringe} is fitted to the data, and the energy and spatial properties remain unchanged.

The CRINGE model fits the cosmic ray flux considering cosmic-ray data from various experiments and combines the best-fit parameters with assumptions about the source distribution, the cross-section, and the photon background in the galactic plane. The result is a model of the diffuse neutrino emission from the galactic plane for an energy range of 10 GeV to 10 PeV [16].

The CRINGE neutrino flux is given in galactic coordinates as it is shown in Figure 4.2. The model is visualized by a Mollweide projection using the python package `healpy`. A Mollweide projection is used to depict a celestial sphere in a two-dimensional map with equal areas [17]. In the center of the map, the neutrino emission of the galactic plane is visible.

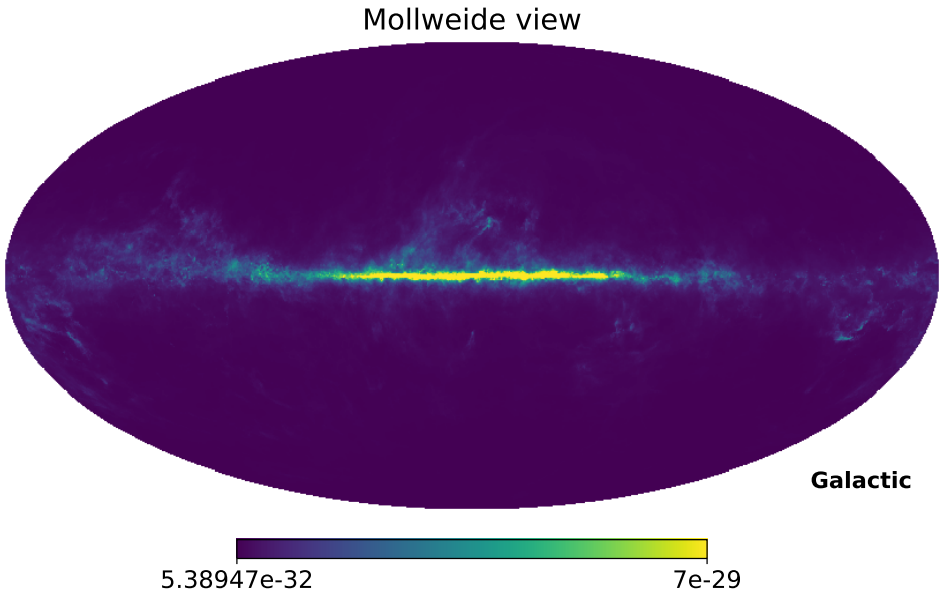

Figure 4.2: CRINGE neutrino flux in galactic coordinates, plotted with `healpy` in Mollweide projection. In the center, the modeled neutrino emission from the galactic plane is shown.

With `healpy`, the coordinate system of the CRINGE model can be changed. This needs to be done for further analysis with neutrino telescopes located on the Earth. For these analyses, Equatorial coordinates are used. The galactic plane in Equatorial coordinates is depicted in Figure 4.3.

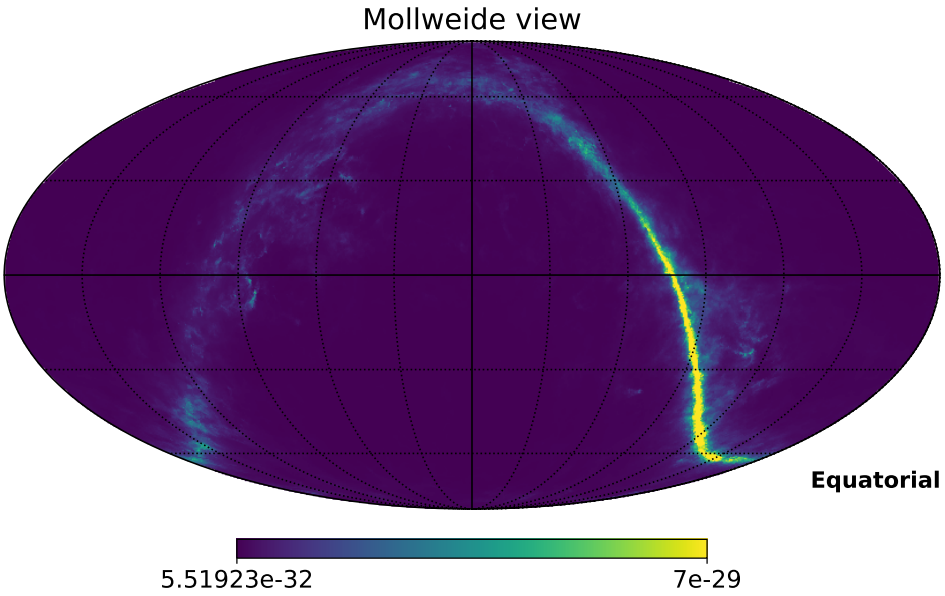

Figure 4.3: CRINGE neutrino flux in Equatorial coordinates, plotted with `healpy` in Mollweide projecetion. The galactic center is located in the southern hemisphere.

The galactic center is located in the southern sky, so the densest part of the galactic plane can only be seen from the southern hemisphere on Earth. As shown in Figure 4.3 also the main part of the expected neutrino flux is coming from the southern hemisphere [15].

5 Analysis Method

The goal of the analysis in this thesis is to identify a significant contribution of the neutrino flux from the galactic plane in public IceCube data. To do this, the PLEnuM framework must be adapted so that the CRINGE flux model is included and the neutrino flux model is fitted to the data.

The total expected neutrino flux is modeled by three neutrino flux components in the following analysis: The atmospheric background, the diffuse (extra-galactic) astrophysical flux, and the diffuse galactic flux. These components are analyzed using a three-dimensional binning: Energy, declination, and right ascension. The energy and declination dependence of the neutrino flux is discussed in subsection 3.2. Especially to distinguish the astrophysical flux from the atmospheric background, the energy distribution needs to be considered. Astrophysical events have high-energy signatures where they dominate over the atmospheric background. Additionally, the declination needs to be included to analyze the galactic plane. The galactic neutrino flux has a distinct structure in the right ascension in comparison to the isotropic atmospheric background due to the Earth's rotation and the diffuse extra-galactic flux.

Each neutrino flux component in the model has a normalization parameter Φ_{model}. Whereas the diffuse flux model has an additional spectral index γ_{astro} as a free parameter. The flux models are fitted to measured detector data. For that, the time-integrated modeled number of neutrino events N_{model} (N_{cringe}, $N_{\text{background}}$ and N_{diffuse}) in IceCube are calculated from the flux models as described in the following. The binned maximum likelihood method then fits the total number of modeled neutrino events. It includes the hypothesis μ with up to four free parameters and the reconstructed neutrino events from detector data k.

Finally, a hypothesis test is used to conclude whether the background hypothesis $H_0(\mu = \{\Phi_{\text{background}}, \Phi_{\text{diffuse}}, \gamma_{\text{astro}}\})$, without the CRINGE model, can be rejected in favor of the signal hypothesis $H_1(\mu = \{\Phi_{\text{cringe}}, \Phi_{\text{background}}, \Phi_{\text{diffuse}}, \gamma_{\text{astro}}\})$, including all flux models. If the background hypothesis can be rejected with high significance, a galactic neutrino flux contribution in the dataset is confirmed.

5.1 Binning

Before this thesis, the input in PLEnuM were only binned in two dimensions: Energy and declination. The input arrays are the effective area determined by Monte Carlo simulations, the simulated background flux, and the isotropic diffuse flux modeled by a power law. The implementation of the additional third dimension, the right ascension α, will be explained in section 6.

The energy is binned in regular bins of the logarithmic energy scale $\log_{10}(E_\nu)$. The declination bins are regular bins in $\sin(\delta)$. Figure 5.1 serves as an example of different binnings, showing the implementation of the simulated atmospheric flux in PLEnuM.

To perform further analysis, it is necessary to select bin sizes. Therefore, a function has been implemented that allows the modification of the binning of all input data. In that function, the `SciPy Regular GridInterpolator` is used to perform linear interpolation over all dimensions of the input data. Once the interpolation is completed, a new grid size is be selected. For instance,

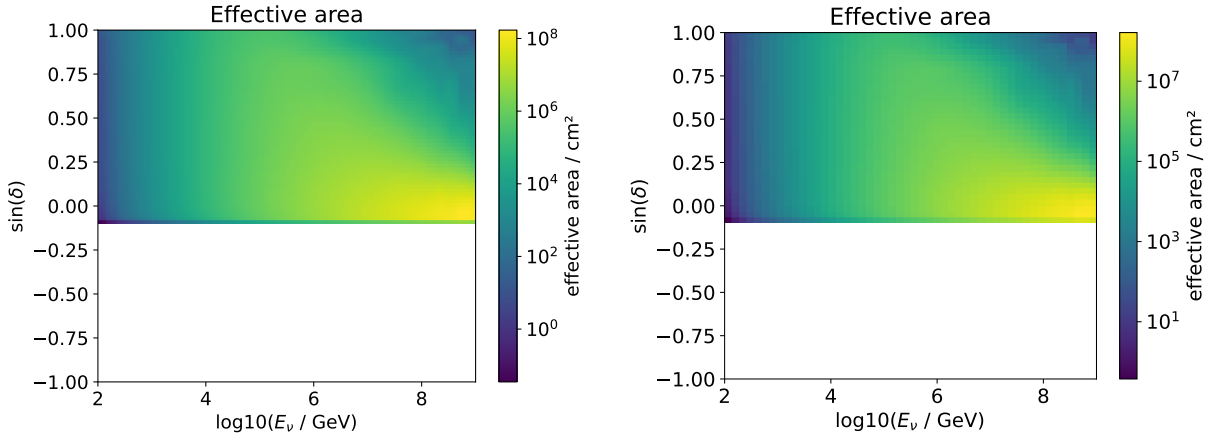

(a) (b)

Figure 5.1: Different energy and declination binning for the effective area. (a) is binned in 140 energy bins and 100 declination bins, as already implemented in PLEnuM. In (b) the binning was modified to larger bins: 30 in energy and 20 in declination. In both cases, the energy range is from 10^2 GeV to 10^9 GeV and is plotted, using a logarithmic scale $\log_{10} E_\nu$. The full declination is displayed in $\sin(\delta)$.

in Figure 5.1 for plot (b), a bin size of 30 energy bins and 20 declination bins are selected. This function is also applicable to three-dimensional binned data, which is important for further analysis of the galactic plane.

5.2 Event Number Determination from Neutrino Flux

This analysis aims to calculate the number of expected neutrinos per bin in the IceCube detector. This calculation is done using the expected neutrino flux for each neutrino flux component. In general, the number of neutrinos N_ν that is expected to be detected at a certain flux $\frac{\mathrm{d}\Phi}{\mathrm{d}E}(E, \delta, \alpha)$ is calculated by [14]:

$$N_\nu = T_{\text{live}} \cdot \int_{\Delta\Omega} \mathrm{d}\Omega \int_{E_{\min}}^{E_{\max}} \mathrm{d}E \, A_{\text{eff}}(E, \sin(\delta), \alpha) \cdot \frac{\mathrm{d}\Phi}{\mathrm{d}E} \tag{5.1}$$

The number of expected events is then compared to the number of measured events for further analysis. Using finite binning for the energy, declination, and right ascension, the integrals are approximated by the bin width. The integrated spatial volume $\mathrm{d}\Omega = \mathrm{d}\alpha\,\mathrm{d}\sin(\delta)$ is be approximated by $\int_{\Delta\Omega} \mathrm{d}\Omega = \Delta\alpha \cdot \Delta\sin(\delta)$ and the integrated energy E by $\int_{E_{\min}}^{E_{\max}} \mathrm{d}E = \Delta E$. The lifetime T_{live}, the timescale covered in the dataset, must also be considered.

For a specific experiment, the binned effective area $A_{\text{eff}}(E, \delta, \alpha)$ is fixed for all neutrino flux contributions. Consequently, a constant factor is defined as:

$$A_{\text{eff.}}^{\text{factor}} = T_{\text{live}} \cdot 2\pi \cdot \Delta\sin(\delta) \cdot \Delta E \cdot A_{\text{eff}}(E, \sin(\delta), \alpha) \tag{5.2}$$

This factor is used for all flux models to calculate the number of expected events binned in three dimensions:

$$N_\nu^{\text{binned}}(E, \sin(\delta), \alpha) = A_{\text{eff.}}^{\text{factor}} \cdot \frac{\mathrm{d}\Phi}{\mathrm{d}E}(E, \sin(\delta), \alpha) \tag{5.3}$$

However, to obtain the energy distribution of the expected neutrino events and the energy distribution of the reconstructed neutrino events in the detector, the energy resolution of the detector needs to be considered. The energy resolution gives a matrix that connects the energy of the detectable muon and the energy of the neutrino as it is shown in Figure 5.2. The fluctuation of the energy resolution is a result of the muons losing energy on their path after their creation [11]. That is why the energy resolution for higher energetic neutrino events is worse, as the muon travels on a longer track, loosing more energy. Multiplying this matrix by the number of expected event bins in the energy dimension enables to compare the result of the matrix product to neutrino reconstructions from detector data.

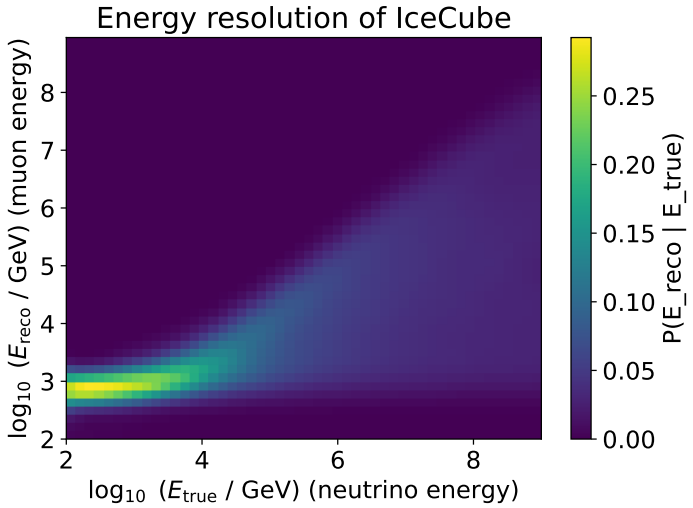

Figure 5.2: The energy resolution considers uncertainties of the energy resolution of a neutrino reconstructed from detector data. For low energies, the energy resolution is more precise than for higher energetic events.

When changing the bin sizes within the analysis, the bin size of the true energy axis in the energy resolution matrix has to change as well.

For each dimension axis, histograms are plotted to illustrate the total neutrino flux. For that, all bins of one model are summed over the other two axes. The modeled event numbers are plotted over energy, declination, and in the further analysis over right ascension. To visualize the total event number from the models, the binned events of different flux models are plotted above each other. An example of the energy axis is shown in Figure 5.3.

5.3 Binned Maximum Likelihood Method

A binned maximum likelihood method is used to fit the binned neutrino flux models to reconstructed detector data. The fit should be performed such that the sum of model event numbers closely matches the measured event numbers.

The likelihood function is defined as the product over all bins with index l, m, n of the Poisson distribution of the data k given the hypothesis μ [14]:

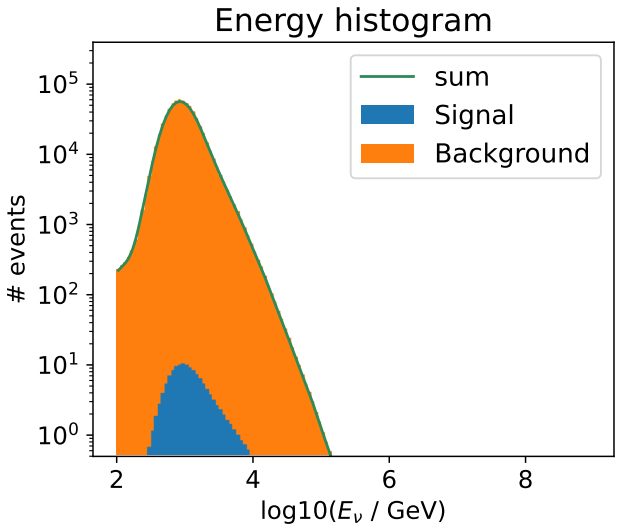

Figure 5.3: Example for an event number histogram for the energy axis. The modeled event numbers for a signal and background models are plotted over the energy in a certain binning. In this plot a binning (140, 100, 50) is used. The background event numbers are plotted above the signal event numbers such that the sum of the two flux components represents the total flux in each energy bin.

$$\mathcal{L}(\text{data}\, k \,|\, \text{hypothesis}\, \mu) = \prod_{\text{bin}\, l,m,n}^{N_{\text{bins}}} \frac{\mu_{lmn}^{k_{lmn}}}{k_{lmn}!} \cdot \exp(-\mu_{lmn}) \tag{5.4}$$

The best-fit of the free hypothesis parameters $\Phi_{\text{cringe}}, \Phi_{\text{background}}, \Phi_{\text{diffuse}}$ and γ_{astro} are obtained by maximizing the likelihood function. However, for numerical stability, it is better to minimize the log-likelihood function $-2 \ln \mathcal{L}(\, k \,|\, \mu)$.

5.4 Profile Likelihood Functions

Profile likelihood functions are statistical tools to determine uncertainties on the best-fit model parameter. The profile likelihood function is calculated depending on one or two model parameters. The function provides a confidence interval for one model parameter and a confidence contour for two parameters. It is visualized by plotting the function for one model parameter or a profile likelihood landscape in two dimensions.

For a given model parameter, the profile likelihood function is calculated by iterating numerically over a certain range of that model parameter. In each iteration step, the corresponding model parameter is used as fixed input into the log-likelihood function. In contrast, all other model parameters of the log-likelihood function are treated as free parameters. The `SciPy` minimizer `fmin_l_bfgs_b` is then used to minimize the log-likelihood depending on the free model parameter in each iteration step. Each of these steps provides one point in the profile likelihood plot, depending on the fixed model parameter. Using small iteration steps, e.g. small differences between the fixed model parameters, results in an almost continuous profile likelihood function.

The minimum of that function then gives the best-fit model parameter. This method allows to determine the confidence interval of the best-fit value.

By iterating over two model parameters, the profile likelihood function depending on these parameters is determined. It is then visualized as the profile likelihood landscape. The minimum in this function also gives the best-fit values for the two model parameters. Around that point, the confidence contours are plotted.

5.5 Hypothesis Testing

The background hypothesis $H_0(\{\mu = \Phi_{\text{background}}, \Phi_{\text{diffuse}}, \gamma_{\text{astro}}\})$ includes only the diffuse and background flux, without the CRINGE model. The signal hypothesis additionally contains the tested signal, the CRINGE model: $H_1(\mu = \{\Phi_{\text{cringe}}, \Phi_{\text{background}}, \Phi_{\text{diffuse}}, \gamma_{\text{astro}}\})$.

To conclude the statistical significance, the signal hypothesis H_1, the maximum likelihood fit including the CRINGE model, is tested against the background hypothesis H_0, the maximum likelihood fit without galactic distribution. A test statistic TS is defined for this purpose [14]:

$$TS = -2\log\left(\frac{H_0(\hat{\mu})}{H_1(\hat{\hat{\mu}})}\right) \tag{5.5}$$

Wilk's theorem states that for a large data sample, which is approximately the case here, TS is χ^2 distributed. The difference in number of fit parameters of the two hypotheses is defined as the number of degrees of freedom of the χ^2 distribution. Therefore a χ^2 distribution with one degree of freedom must be used [3].

The null hypothesis H_0 is rejected for a certain p-value $p < \alpha$, corresponding to a certain significance level α. Usually $\alpha = 2.9 \cdot 10^{-7}$ is chosen. This corresponds to a $5\,\sigma$ significance level. The p-value is determined by integrating over the χ^2 distribution [3]:

$$1 - p = \int_0^{TS} f_{\chi^2} \mathrm{d}\chi^2 \tag{5.6}$$

The significance Z gives the deviation from the Gaussian mean corresponding to the p-value:

$$\int_{-\infty}^{Z} N(z; \mu = 0, \sigma^2 = 1)\,\mathrm{d}z = 1 - p \tag{5.7}$$

where N is the normal distribution with mean μ and variance σ^2.

6 Analysis on the Galactic Plane

6.1 Three Dimensional Binning

When analyzing the galactic plane it is necessary to consider all models and data in three dimensions. However, the analyses in PLEnuM for point-sources and the diffuse astrophysical flux were previously conducted in a two-dimensional binning that included energy and declination. The two-dimensional arrays containing the models have the shape (# energy bins , # declination bins). Therefore the right ascension axis must be implemented to analyze the galactic plane.

The binning of the effective area needs to be changed to a three-dimensional binning. The correct binning in $A_{\text{eff.}}^{\text{factor}}$ allows to calculate the number of modeled neutrino events N_ν. This binning array has the shape (# energy bins , # declination bins, # right ascension bins). The effective area is uniform in right ascension. This allows to divide every bin in energy and declination by the number of right ascension bins. Every right ascension bin with equal energy and declination contains this value. Therefore the sum over the right ascension axis in three dimensions, for a certain energy and declination, has to have the same value as evaluating the two-dimensional array at the same energy and declination. The effective area in the three-dimensional binning is shown in Figure 6.1.

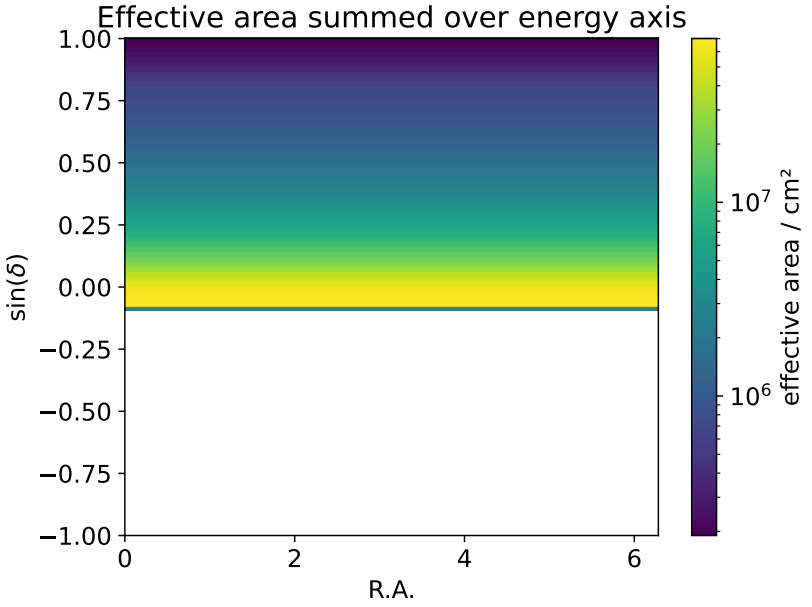

Figure 6.1: Three-dimensional binned effective area in declination $\sin(\delta)$ and right ascension $R.A.$ summed over the energy axis. The right ascension axis has a range of 2π. The effective area is implemented uniformly in right ascension.

Additionally, the background model and the diffuse flux model must be rebinned. As both models are also uniform in right ascension, the rebinning works as implemented for the effective area. The modeled event numbers for the neutrino background and diffuse flux are then determined as described in section 5. It is visualized by histograms in each bin axis, as it is plotted in Figure 6.2 for the diffuse and atmospheric background model. The total number of events has to

be kept constant in two and three dimensions for each model. For the models used in this thesis in total 1,968 diffuse neutrino events and 439,699 atmospheric background neutrino events are considered.

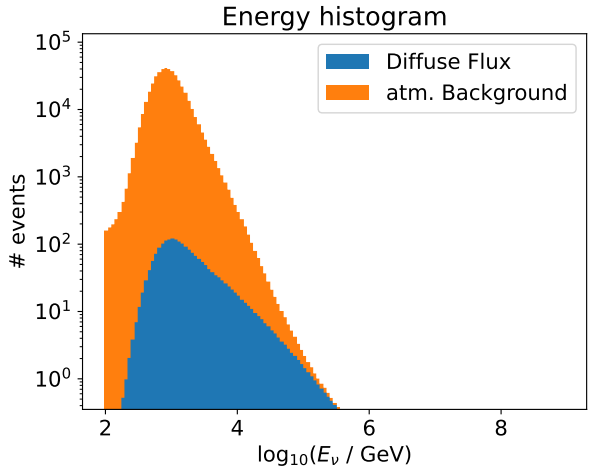

(a) energy

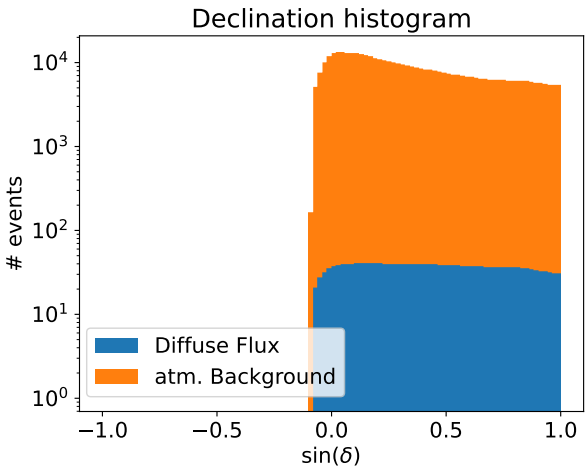

(b) declination

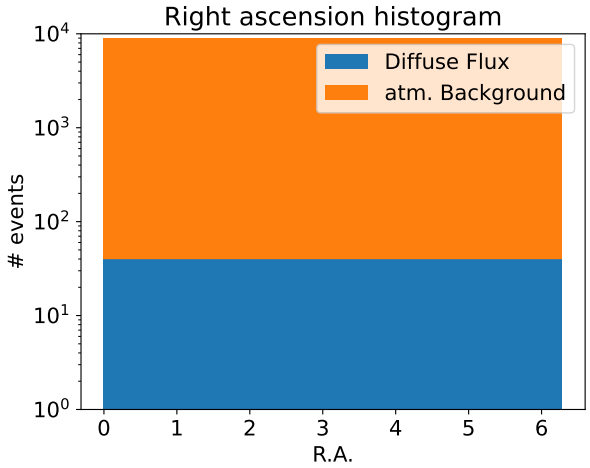

(c) right ascension

Figure 6.2: Histograms of modeled neutrino events per bin summed over three bin axes each: (a) energy, (b) declination, and (c) right ascension. In these histograms, the atmospheric background and the diffuse flux model are included. The number of atmospheric background events is plotted above the diffuse flux events, so the sum of both flux contributions is directly visible in the plots.

6.2 Analysis with the CRINGE Model

In order to draw conclusions about the galactic plane, the implementation of the CRINGE model, which is a galactic plane model, is necessary.

6.2.1 Implementation of the CRINGE model

The implementation of the CRINGE model is done in galactic coordinates. As mentioned in subsection 2.3, the coordinate system is changed to equatorial coordinates with `healpy`. However, one problem is that this modeled flux is not given in coordinates on a sphere. To obtain the CRINGE neutrino flux in correct binning, a Spline is needed which integrates over the whole data set. After that, a rebinning in equal-sized energy, declination, and right ascension in spherical coordinates is possible. To obtain the correct CRINGE flux, Georg Schwefer[1] implemented a function that was used in this thesis. The binned CRINGE flux is shown in Figure 6.3. The CRINGE flux contributes 91 neutrino events to the total modeled neutrino flux in the baseline CRINGE model with $\Phi_{\text{cringe}} = 1$.

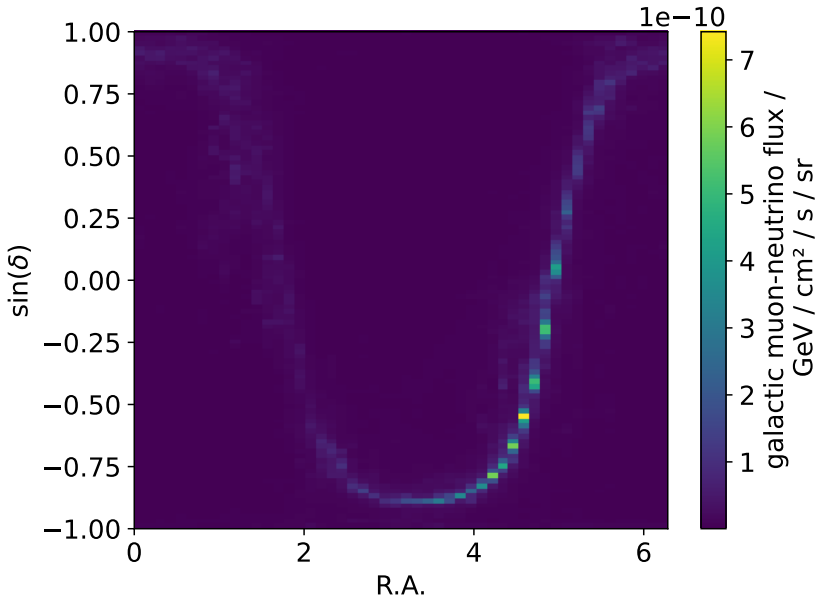

Figure 6.3: The CRINGE flux is binned in three axes as the other neutrino flux models. Here the distinct structure of the diffuse galactic flux in the right ascension axis is shown.

The number of modeled galactic plane neutrinos is determined from the CRINGE flux as described in subsection 5.2. So this flux component is added to the model histograms as it is shown for example in Figure 6.4. In this plot a binning $(\#\,\text{energy bins}, \#\,\text{declination bins}, \#\,\text{right ascension bins}) = (140, 100, 50)$ is used. Figure 6.4 (c) shows the unique shape of the CRINGE flux in right ascension in comparison to the uniform background and diffuse flux.

6.2.2 Fit on Modeled Data

To test the implementation of the CRINGE model, a maximum likelihood fit is performed on simulated total neutrino flux data. Each flux model contributes to the total neutrino flux. So by assuming a value for the model's parameters individual event numbers are obtained. These event

[1] private communication

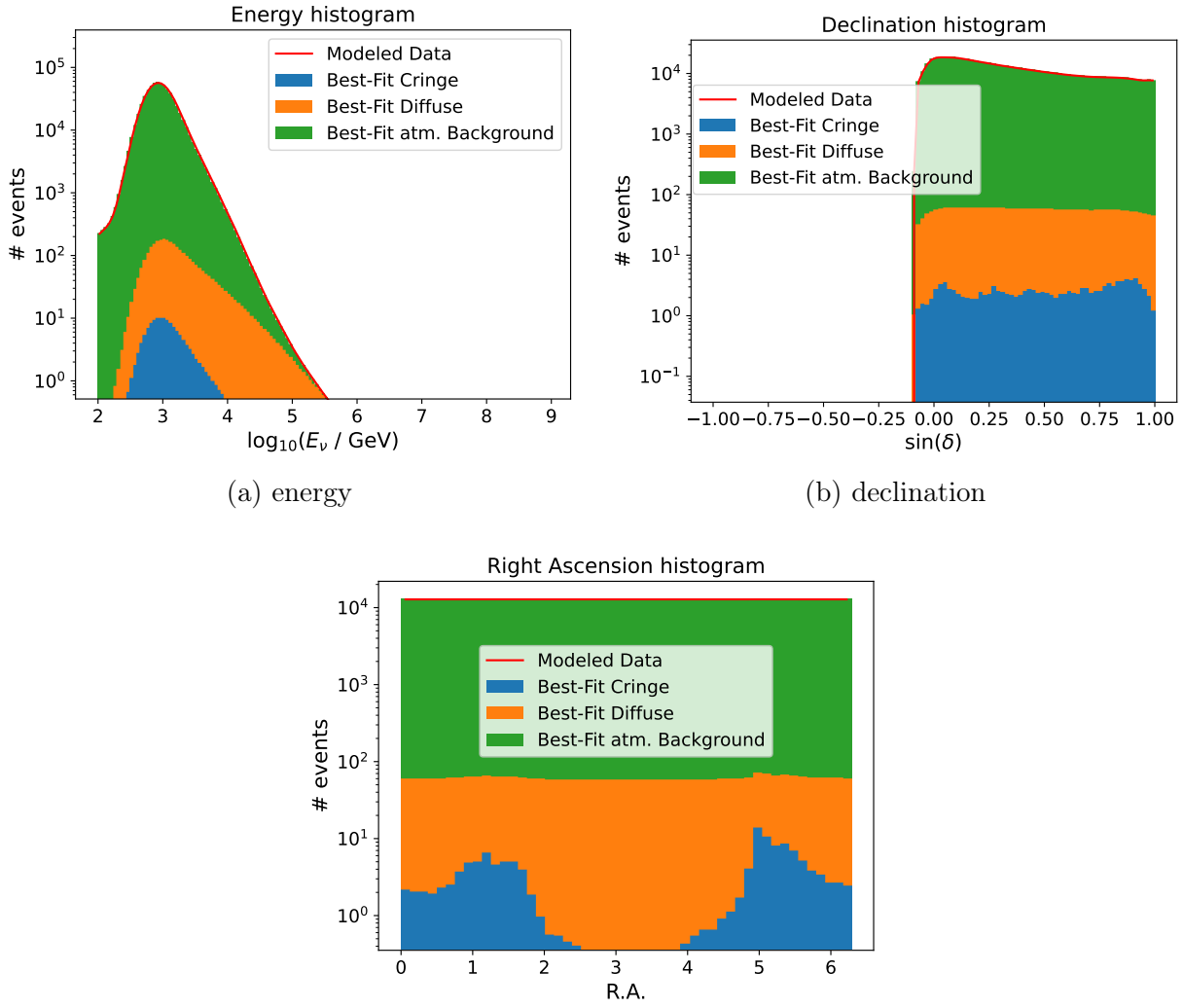

(a) energy

(b) declination

(c) right ascension

Figure 6.4: Histograms of best-fit modeled neutrino events per bin summed over three bin axes each: (a) energy, (b) declination, and (c) right ascension fitting the simulated data shown in red. The best-fit parameters are $\Phi_{\text{background}}^{\text{model best-fit}} = \Phi_{\text{diffuse}}^{\text{model best-fit}} = \Phi_{\text{cringe}}^{\text{model best-fit}} = 1.00$ for the normalization parameters and $\gamma_{\text{astro}}^{\text{model best-fit}} = 2.30$ for the spectral index.

numbers of the neutrino flux models in every bin are added to obtain a total neutrino flux model dataset.

In the following, the normalization factor for the atmospheric and diffuse model is set to $\Phi_{\text{background}} = \Phi_{\text{diffuse}} = 1$. The analysis of the IceCube collaboration on the galactic plane using the CRINGE number predicts a higher CRINGE normalization than $\Phi_{\text{cringe}} = 1$. The CRINGE normalization is chosen based on the analysis of Philipp Fürst [8] to $\Phi_{\text{cringe}} = 3$. Therefore the CRINGE model in the maximum likelihood function is also obtained with a factor of three. The spectral index is based on the same IceCube analysis where the diffuse flux is also modeled by a power-law. So the spectral index is set to $\gamma_{\text{astro}} = 2.3$ [8]. In this model 637,286 atmospheric background

events, 2,852 diffuse astrophysical neutrino events, and 398 galactic neutrino events contribute to a dataset, containing 640,535 neutrino events, in total.

In a fit of the neutrino flux components to this model, the expected best-fit model parameters are $\Phi_{\text{background}} = \Phi_{\text{diffuse}} = \Phi_{\text{cringe}} = 1.00$ for the normalization parameters and $\gamma_{\text{astro}} = 2.30$ for the spectral index. In Figure 6.4, the model dataset is shown as a red line in each axis. The neutrino flux models are fitted to that dataset. The best-fit model parameters are obtained to $\Phi_{\text{background}}^{\text{model best-fit}} = 1.00$, $\Phi_{\text{diffuse}}^{\text{model best-fit}} = 1.00$, $\gamma_{\text{astro}}^{\text{model best-fit}} = 2.38$ and $\Phi_{\text{cringe}}^{\text{model best-fit}} = 1.00$ as expected and fit the model data.

To investigate the uncertainties of the best-fit model parameters, profile likelihood plots are considered. For the CRINGE normalization, a clear minimum is found in the profile likelihood function (cf. Figure 6.5). The uncertainties of the best-fit model parameter are determined to $\Phi_{\text{cringe}} = 1.00^{+0.79}_{-0.79}$.

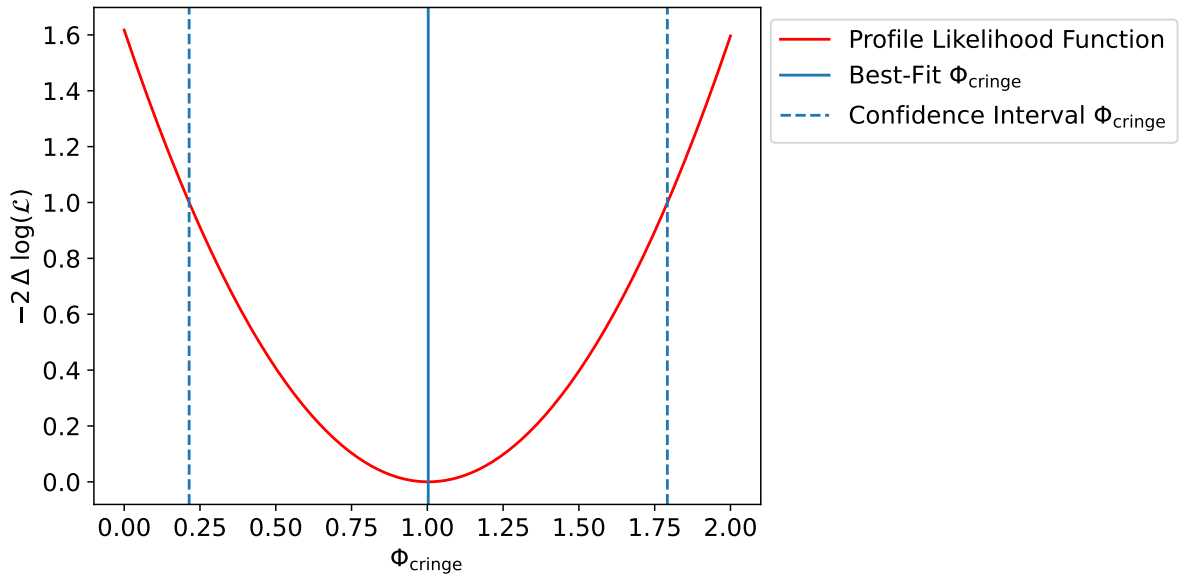

Figure 6.5: Profile likelihood function depending on the cringe normalization parameter Φ_{cringe}. The profile likelihood function has a minimum at $\Phi_{\text{cringe}} = 1.00$, which corresponds to the best-fit cringe normalization value. The uncertainties of the normalization are determined to $\Phi_{\text{cringe}} = 1.00^{+0.79}_{-0.79}$.

Uncertainties of the CRINGE normalization parameter corresponding to the other model parameters are investigated via profile likelihood landscapes as shown in Figure 6.6. The confidence contours are only slightly tilted. Therefore, Φ_{CRINGE} is marginally correlated to the other fit parameters. The extension of the confidence contour on the CRINGE axis is larger than on the axis of the corresponding parameter. This is due to a higher contribution of the other flux models to the total modeled neutrino flux.

The significance of the rejection of a neutrino flux model without the CRINGE distribution is determined via a hypothesis test. The signal hypothesis $H_1(\mu = \{\Phi_{\text{cringe}}, \Phi_{\text{background}}, \Phi_{\text{diffuse}}, \gamma_{\text{astro}}\})$, including the CRINGE model, is tested against the background hypothesis $H_0(\mu = \{\Phi_{\text{background}}, \Phi_{\text{diffuse}}, \gamma_{\text{astro}}\})$, without the CRINGE model as described in subsection 5.5. The result is a p-

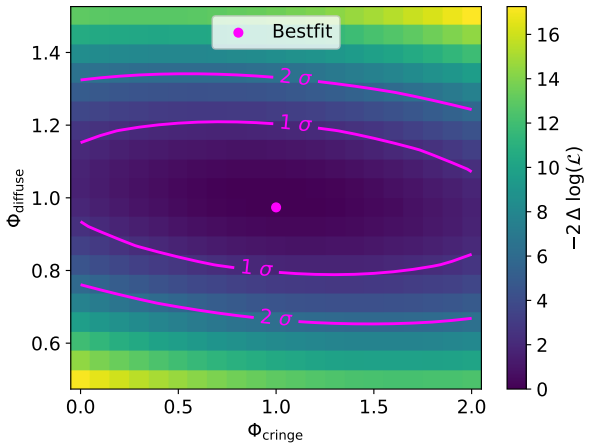

(a) Profile likelihood Φ_{cringe}-Φ_{diffuse}

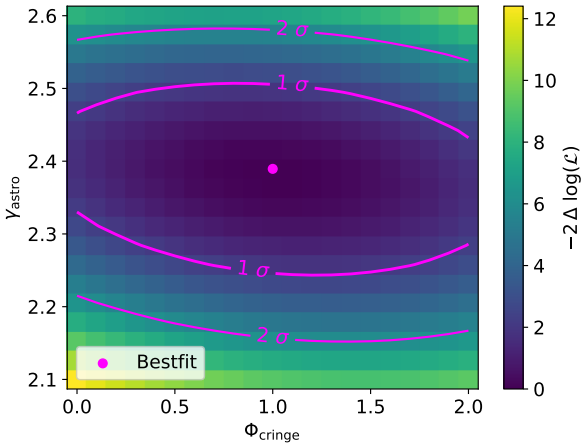

(b) Profile likelihood Φ_{cringe}-γ_{astro}

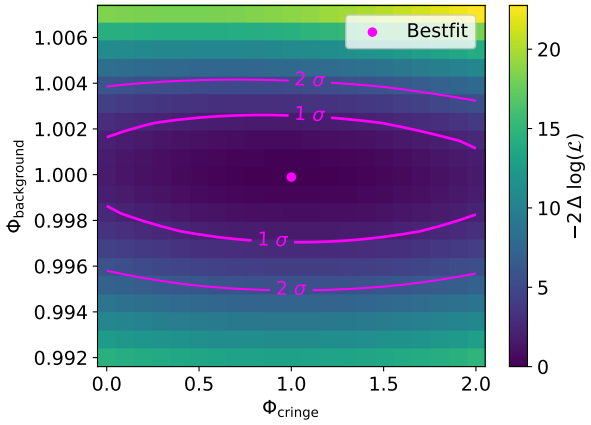

(c) Profile likelihood Φ_{cringe}-$\Phi_{\text{background}}$

Figure 6.6: Profile likelihood landscape for the cringe normalization parameter Φ_{cringe} combined with a different model parameter in each plot. The fit is performed on a modeled dataset. Figure (a) - (c) contain the best-fit parameter, the minimum in the profile likelihood landscape, the $1\,\sigma$, and $2\,\sigma$ contour.

value of $p = 0.20$. So the background hypothesis is rejected with a significance of $0.83\,\sigma$ for the model dataset.

This low significance can be explained by the limited contribution of the CRINGE model to the overall neutrino flux. The CRINGE model is responsible for only 398 neutrino events out of the $640,535$ total events in the modeled dataset. Given that the neutrino flux models are exactly contained within the dataset, a significance higher than $0.83\,\sigma$ is not expected when testing the CRINGE model on IceCube data.

6.3 Fit on IceCube Data

Public IceCube data are used for the CRINGE model's significance test. This dataset needs to be prepared to have the same dimensions and binning as the modeled data. After that, the fit on the modeled data is performed.

6.3.1 IceCube Data Release

The IceCube dataset used in the following is from the public data release for all-sky point like neutrino sources including 10 years of data (2008 – 2018). This data release contains selected track-like events originating primarily from muon neutrinos. Before 2012 the event selection was not standardized. In the years after, the event selection called `PSTracks` was updated which improved the sample sensitivity. That is why only data samples after the update are used in this thesis. These datasets are labeled IC86-II to IC86-VII for each year between April 2012 and May 2018. So six years of the data with a total of 537,841 selected neutrino events are included [10].

The events selection `PSTracks` is performed to identify high-energy muons passing the detector to identify astrophysical neutrinos. For northern and southern hemisphere events different selection criteria are applied. However, for this analysis, only events from the northern hemisphere are considered. As mentioned in section 3, the atmospheric muons from the northern sky are filtered by the Earth. There are still some atmospheric muons reaching the detector that are incorrectly reconstructed into the northern sky. Therefore only high-quality track-like events are used. To optimize the selection since the data IC86-II release a Boosted Decision Tree is used to classify events into muon tracks from atmospheric and astrophysical neutrinos, atmospheric muons, and cascades. With that algorithm, 90% of atmospheric neutrinos and 0.1% of atmospheric muons from the high-quality track-like events are preserved [10].

6.3.2 Prepare IceCube Data

After importing the IceCube neutrino events, the data must be binned in three dimensions. The choice of bin size is based on the galactic diffuse flux analysis using northern tracks by Philipp Fürst. Within his analysis, a binning of (# energy bins , # declination bins, # right ascension bins) = $(50, 33, 180)$ is used. For the analysis in this thesis a binning of (# energy bins , # declination bins, # right ascension bins) = $(50, 60, 180)$ is used. A higher declination binning does contain more information about the event distribution over that axis. As long as a global minimum is reached by the optimizer of the maximum likelihood function, a higher binning can always be chosen.

An all-sky IceCube data release is used which means that also neutrino events from the southern hemisphere are included. Therefore the IceCube data are cut at $\delta = -5°$, as the effective area is assumed to be zero below that angle.

In Figure 6.7 (a) is shown that the accuracy of the fit to IceCube data, including the diffuse flux model and the atmospheric model, decreases for energies below $E_\nu = 10^{2.8}\,\mathrm{GeV}$. This is determined in each bin by calculating the energy ratio $\frac{\text{Sum Best–Fit Model}}{\text{IceCube Data}}$ (cf. Figure 6.7 (b)). If the energy ratio $\frac{\text{Sum Best–Fit Model}}{\text{IceCube Data}} = 1$, the total modeled number of neutrino events is fitted to a value equal to the measured events in each bin. The deviation of the fitted event number from

the event number in the dataset is due to an inaccurate model of the atmospheric background in the energy region $E_\nu < 10^{2.8}\,\mathrm{GeV}$ and fluctuations in the dataset. The atmospheric background dominates the high-energy neutrino flux and the model can not be adapted by the fitting process, only the normalization factor can be changed.

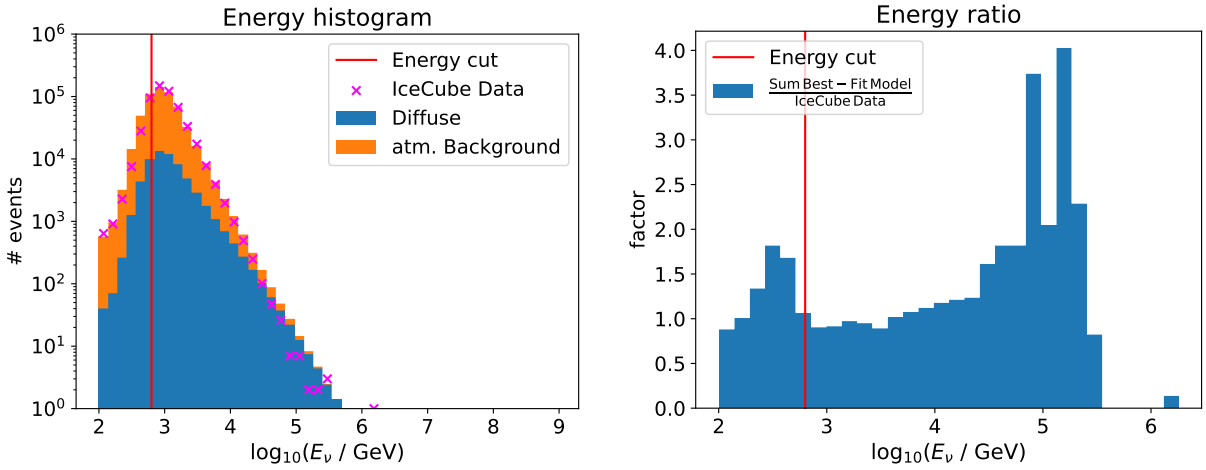

(a) (b)

Figure 6.7: (a) Energy histogram of best-fit diffuse model and best-fit atmospheric background without energy cut, plotted in comparison to the IceCube data. The energy cut will cut all energy bins $E_\nu < 10^{2.8}\,\mathrm{GeV}$, shown by the red line. (b) Energy ratio between $\frac{\text{Sum Best–Fit Model}}{\text{IceCube Data}}$ for determining the energy cut. The energy cut is performed where the ratio is approximately one. So the energy cut, shown by the red line, is drawn at $E_\nu = 10^{2.8}\,\mathrm{GeV}$.

Therefore an energy cut is introduced to the IceCube data. Consequently, also the flux models need an energy cut. The energy cut is set as low as possible to prevent excessive data loss. The energy cut is determined by fitting the diffuse and background model to the data, as shown in Figure 6.8 (a). Only the energy range where the fitted model and the data are approximately equal $\frac{\text{Sum Best–Fit Model}}{\text{IceCube Data}} = 1$ is kept by performing an energy cut. It is shown in Figure 6.8 (b) that an energy cut at $10^{2.8}\,\mathrm{GeV}$ satisfies that requirement. The ratio condition is fulfilled for energies between $10^{2.8}\,\mathrm{GeV}$ and $10^{4.7}\,\mathrm{GeV}$. Higher energies are not considered in this decision as the event rate is very low (maximum 100 events per bin). With the declination, and energy cut 403,014 of the initial 537,841 neutrino events from the IceCube dataset remain.

6.3.3 Fit Model to IceCube Data

In section 5, it is explained that two fits are necessary for the hypothesis test. The first fit involves the background hypothesis, which assumes that there is no galactic contribution to the total neutrino flux: $H_0(\mu = \{\Phi_{\text{background}}, \Phi_{\text{diffuse}}, \gamma_{\text{astro}}\})$. To perform this fit, the normalization parameter of the CRINGE model Φ_{cringe} is set to zero. Therefore, only the atmospheric background and the diffuse flux are fitted. The resulting best-fit histograms for declination and right ascension shown in Figure 6.9. The best-fit energy histogram is shown in Figure 6.8 (a). The best-fit parameter

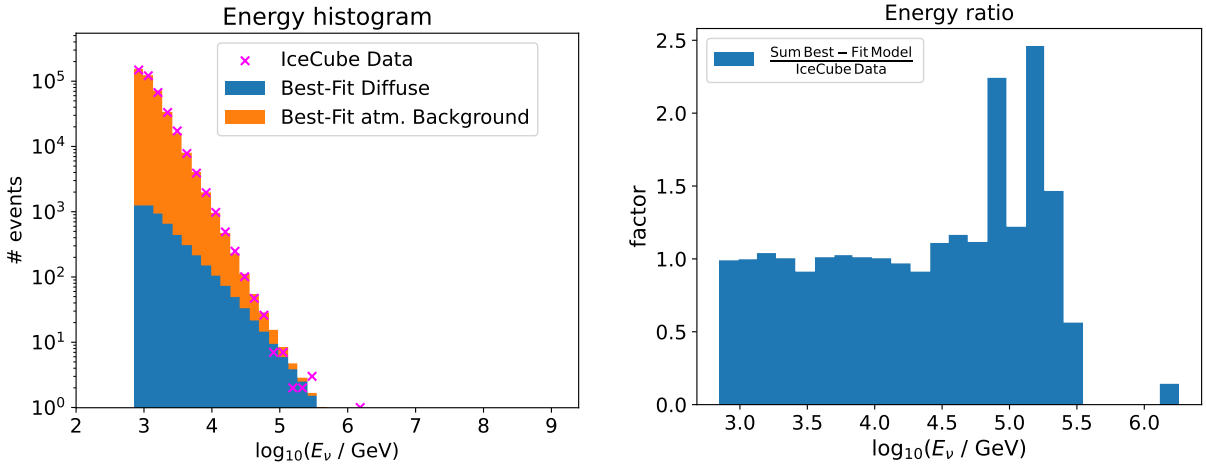

(a) (b)

Figure 6.8: (a) Energy histogram of best-fit diffuse model and best-fit atmospheric background after the energy cut, plotted in comparison to the IceCube data. Before the fitting process, model and data were cut at an energy of $E_\nu = 10^{2.8}\,\mathrm{GeV}$. The fitted model deviates from the IceCube data for energies $E_\nu > 10^{4.7}\,\mathrm{GeV}$. (b) Energy ratio between $\frac{\text{Sum Best−Fit Model}}{\text{IceCube Data}}$ for the chosen energy cut at $E_\nu = 10^{2.8}\,\mathrm{GeV}$. For that energy cut, the ratio is approximately one for all energy bins, except for high energies, $E_\nu > 10^{4.7}\,\mathrm{GeV}$.

for the background normalization $\Phi^{\text{best−fit}}_{\text{background}} = 1.30$ and for the diffuse flux $\Phi^{\text{best−fit}}_{\text{diffuse}} = 2.23$ are obtained. The spectral index of the diffuse flux is fitted to $\gamma^{\text{best−fit}}_{\text{astro}} = 2.54$.

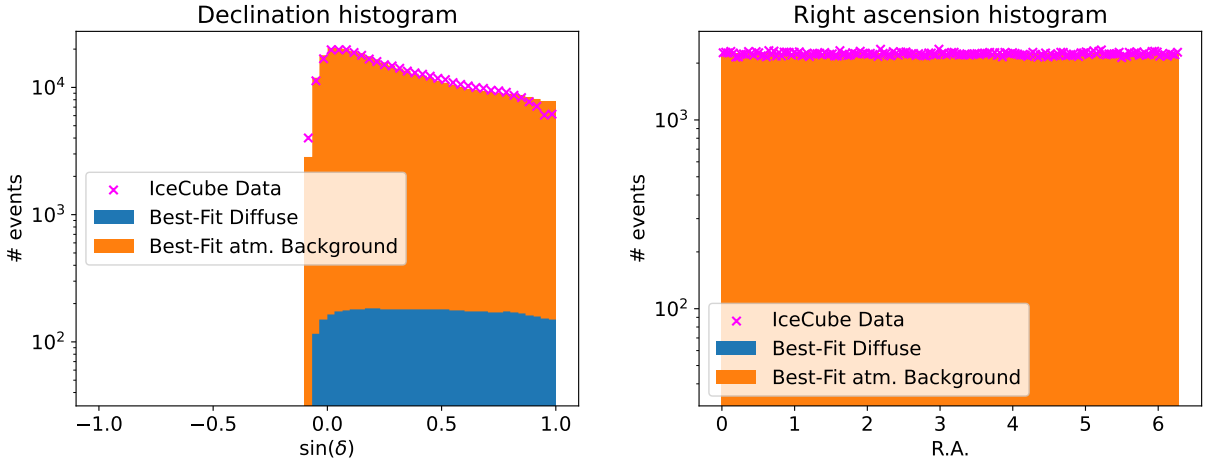

(a) (b)

Figure 6.9: (a) Declination histogram of best-fit diffuse model and best-fit atmospheric background plotted in comparison to the IceCube data. Before the fitting process, model and data were cut in declination at $\delta = -5°$. The fit in declination deviates from IceCube data for angles close to $\delta = 90°$. (b) Right ascension histogram of best-fit diffuse model and best-fit atmospheric background plotted in comparison to the IceCube data.

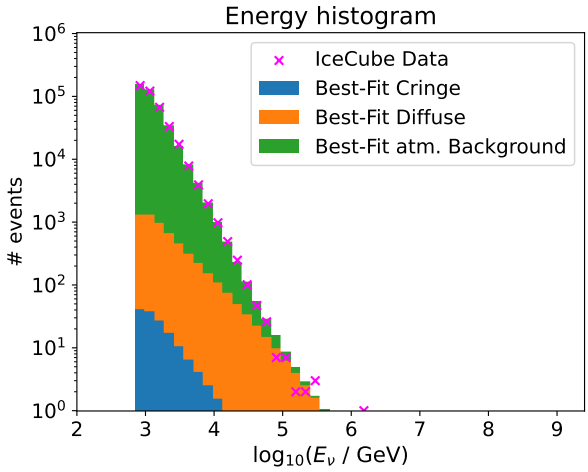

(a) energy

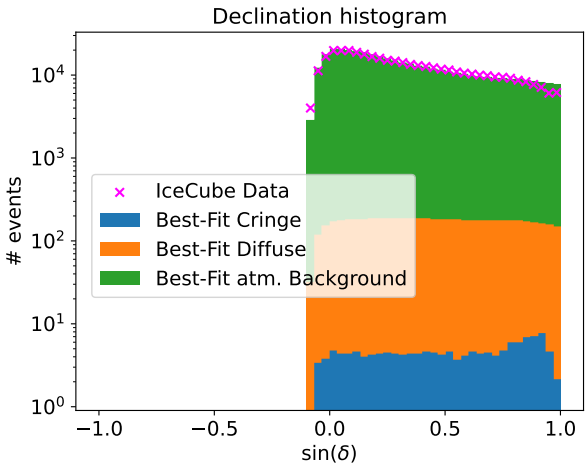

(b) declination

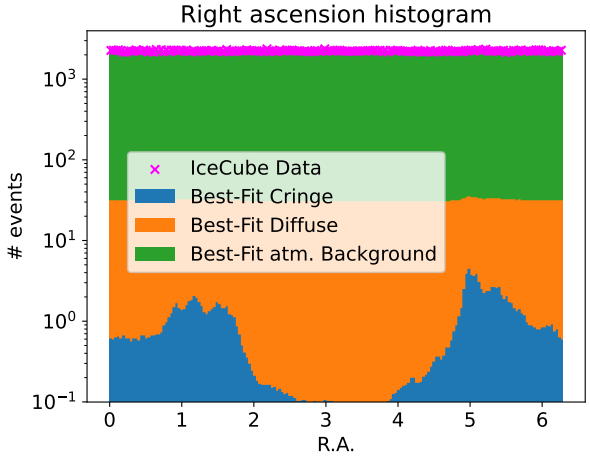

(c) right ascension

Figure 6.10: Best-Fit models including CRINGE flux, diffuse astrophysical flux, and background flux in comparison to IceCube data. The best-fit normalization parameters are $\Phi^{\text{best-fit}}_{\text{background}} = 1.30$, $\Phi^{\text{best-fit}}_{\text{diffuse}} = 2.20$ and $\Phi^{\text{best-fit}}_{\text{cringe}} = 2.14$. The best-fit spectral index in the diffuse astrophysical flux model is $\gamma^{\text{best-fit}}_{\text{astro}} = 2.54$. (a) The model parameter fits the energy for lower energies. For energies $E_\nu > 10^{4.7}\,\text{GeV}$ the deviation gets larger. (b) The fit in declination deviates from IceCube data for angles close to $\delta = 90°$. This is also observed in the fit, not including the CRINGE model. (c) In the right ascension axis, no larger deviations between the fitted model and IceCube data are observed.

The fit for the signal hypothesis $H_1(\mu = \{\Phi_{\text{cringe}}, \Phi_{\text{background}}, \Phi_{\text{diffuse}}, \gamma_{\text{astro}}\})$ includes the CRINGE neutrino flux. The best-fit parameters are $\Phi^{\text{best-fit}}_{\text{background}} = 1.30$, $\Phi^{\text{best-fit}}_{\text{diffuse}} = 2.20$, $\gamma^{\text{best-fit}}_{\text{astro}} = 2.54$ and $\Phi^{\text{best-fit}}_{\text{cringe}} = 2.14$ shown in Figure 6.10.

6.3.4 Profile Likelihood Plots for Analysis on IceCube Data

After fitting the models of neutrino flux to the IceCube data, it is necessary to consider uncertainties in the determined model parameter. This is done by using profile likelihood plots.

The confidence interval for the cringe normalization parameter is determined by the profile likelihood function shown in Figure 6.11. The uncertainties of the parameter are determined to $\Phi_{\text{cringe}} = 2.14^{+3.61}_{-3.62}$. The $1\,\sigma$ confidence interval reaches the region of unphysical negative values. This problem can be overcome by using the method of Feldmann and Cousins [7] for further analysis. With that method, a confidence interval without reaching unphysical regions can be specified [7].

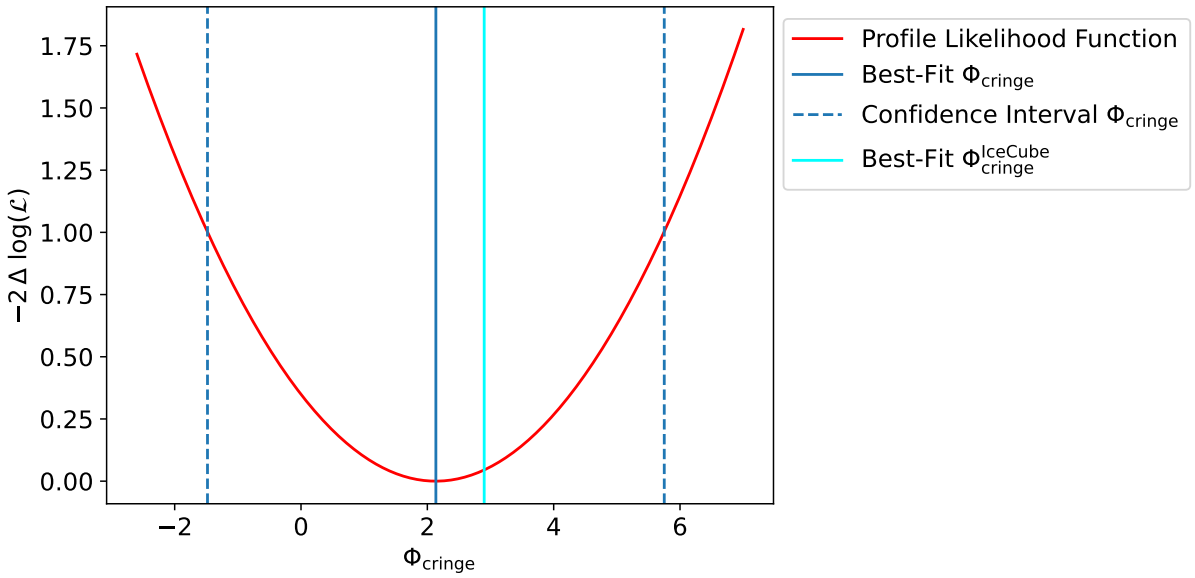

Figure 6.11: Profile likelihood function depending on the cringe normalization parameter Φ_{cringe}. The profile likelihood function has a minimum at $\Phi_{\text{cringe}} = 2.14$, which corresponds to the best-fit cringe normalization value. The uncertainties of the normalization are determined to $\Phi_{\text{cringe}} = 2.14^{+3.61}_{-3.62}$. Within the $1\,\sigma$ confidence interval, unphysical negative values are reached.

The best-fit parameter of the CRINGE normalization $\Phi^{\text{IceCube}}_{\text{cringe}}$ of the same analysis performed by the IceCube collaboration, is located within the confidence interval of this thesis (cf. Figure 6.11). This IceCube analysis and a comparison to the analysis in this thesis are discussed in subsection 7.2.

The correlation of the cringe normalization parameter with the other model parameters is investigated with three profile likelihood landscapes as shown in Figure 6.12. As described above, the confidence interval of the CRINGE flux normalization covers a range from unphysical values $\Phi_{\text{cringe}} < 0$ up to physical values $0 \leq \Phi_{\text{cringe}} \leq 5.76$. This is why the two-dimensional $1\,\sigma$ contour is extended to these values. The tilting of the ellipse marking the $1\,\sigma$ interval depends on whether the two model parameters plotted are correlated. It is tilted in case of a correlation between the model parameter in the profile likelihood function. In the profile likelihood landscapes only a slight tilt is visible. So the model parameters are not strongly correlated.

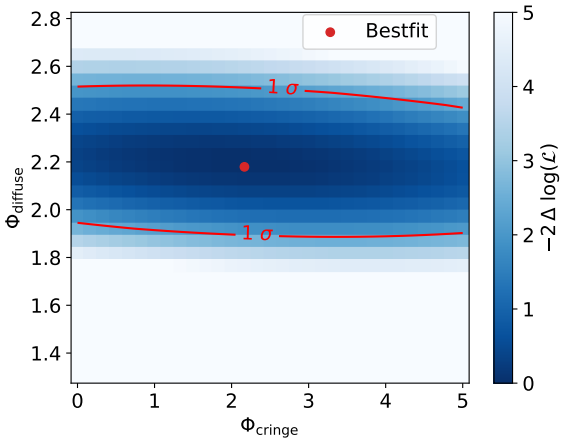

(a) Profile likelihood Φ_{cringe}-Φ_{diffuse}

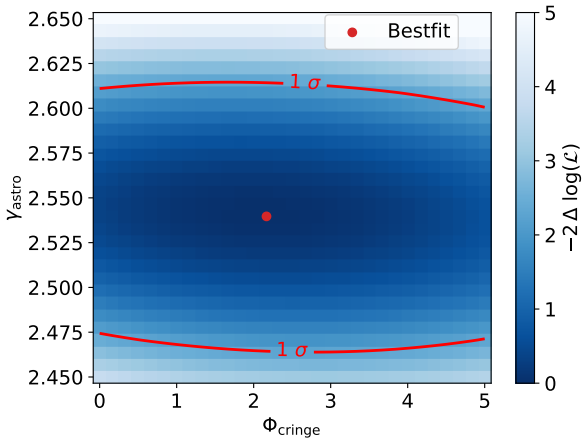

(b) Profile likelihood Φ_{cringe}-γ_{astro}

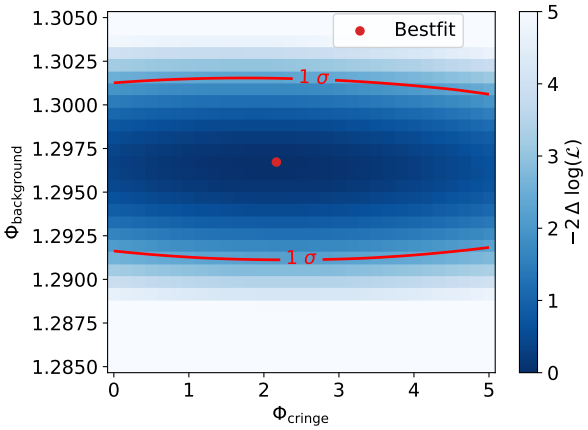

(c) Profile likelihood Φ_{cringe}-$\Phi_{\text{background}}$

Figure 6.12: Profile likelihood landscape for the cringe normalization parameter Φ_{cringe} combined with a different model parameter in each plot. Figure (a) - (c) contain the best-fit parameter, the minimum in the profile likelihood landscape, and the $1\,\sigma$ contour. In all plots, the $1\,\sigma$ contour is only slightly tilted and covers a wide Φ_{cringe} range.

7 Results and Discussion

7.1 Hypothesis Test CRINGE Model

A Hypothesis test as described in subsection 5.5 is performed to decide whether the background hypothesis $H_0(\mu = \{\Phi_{\text{background}}, \Phi_{\text{diffuse}}, \gamma_{\text{astro}}\})$, without the CRINGE model, can be rejected in favor of the alternative hypothesis $H_1(\mu = \{\Phi_{\text{cringe}}, \Phi_{\text{background}}, \Phi_{\text{diffuse}}, \gamma_{\text{astro}}\})$, including the CRINGE model. The test statistic as described in Equation 5.5 is obtained by using the fits from subsubsection 6.3.3. The p-value is calculated via Equation 5.6. The p-value corresponding to the given data is determined to $p = 0.56$. Therefore the background hypothesis can not be rejected in my thesis. This result is consistent with the fit of the flux models to the modeled data set. In that hypothesis test a p-value $p = 0.20$ is obtained and therefore no higher significance on the IceCube data is expected.

One reason for the lack of a significant contribution of the galactic neutrino flux in the public dataset can be that the dataset contains only six years of data. Selecting only data from the northern hemisphere further limits the number of events used in the dataset. By selecting only northern tracks with an energy $E_\nu < 10^{2.8}\,\text{GeV}$, only $403,014$ neutrino events remain. By using a dataset containing a larger timescale of IceCube data, the significance can be improved. For example, the dataset of the galactic plane IceCube analysis using the CRINGE model described in subsection 7.2, contains $982,279$ northern track events.

7.2 Comparison to IceCube analysis of CRINGE Model

Philipp Fürst on behalf of the IceCube Collaboration performed the "Galactic and Extragalactic Analysis of the Astrophysical Muon Neutrino Flux with 12.3 years of IceCube Track Data", presented at the International Cosmic Ray Conference 2023. In this analysis, the CRINGE model was used to model the diffuse neutrino flux from the galactic plane. The IceCube collaboration was able to fit the CRINGE normalization parameter to $\Phi_{\text{cringe}}^{\text{IceCube}} = 2.9 \pm 1.1$ (cf. Figure 6.11). The background hypothesis in this analysis can be rejected with a significance of $2.7\,\sigma$ in favor of the signal hypothesis including a galactic neutrino flux. In this analysis, also only northern track events are used, cutting the data at a declination angle $\delta = -5°$. In contrast to this thesis, a dataset of 12.3 years and events with energies of $10^2\,\text{GeV}$ and higher were considered [8].

The confidence interval of the CRINGE normalization $\Phi_{\text{cringe}}^{\text{IceCube}}$ contains the best-fit parameter $\Phi_{\text{cringe}} = 2.14$ found in this thesis. A normalization factor of $\Phi_{\text{cringe}} = 1$ corresponds to a best-fit of the CRINGE neutrino flux as predicted in the model. As both analyses fit a CRINGE model with $\Phi_{\text{cringe}}^{\text{best-fit}} > 1$, there is a hint that the galactic flux could be higher than predicted by the CRINGE model. This can be the case due to the CRINGE model only including the diffuse galactic neutrino flux and no galactic point-source contribution. The galactic neutrino point-sources can add a significant contribution to the total galactic neutrino flux.

However, the model parameter of the diffuse astrophysical flux differs as shown in Figure 7.1 and Figure 7.2 (a). For the diffuse astrophysical flux in the IceCube Collaboration's analysis also a power law is assumed. Therefore, the model parameters that are obtained, are the same as in this thesis: diffuse flux normalization $\Phi_{\text{diffuse}}^{\text{IceCube}}$ and spectral index $\gamma_{\text{astro}}^{\text{IceCube}}$. These parameters

are determined to $\Phi_{\text{diffuse}}^{\text{IceCube}} = 1.51^{+0.22}_{-0.23}$ and $\gamma_{\text{astro}}^{\text{IceCube}} = 2.38^{+0.08}_{-0.08}$. The likelihood landscape of the parameters from the IceCube Collaboration including the confidence contour is shown in Figure 7.1.

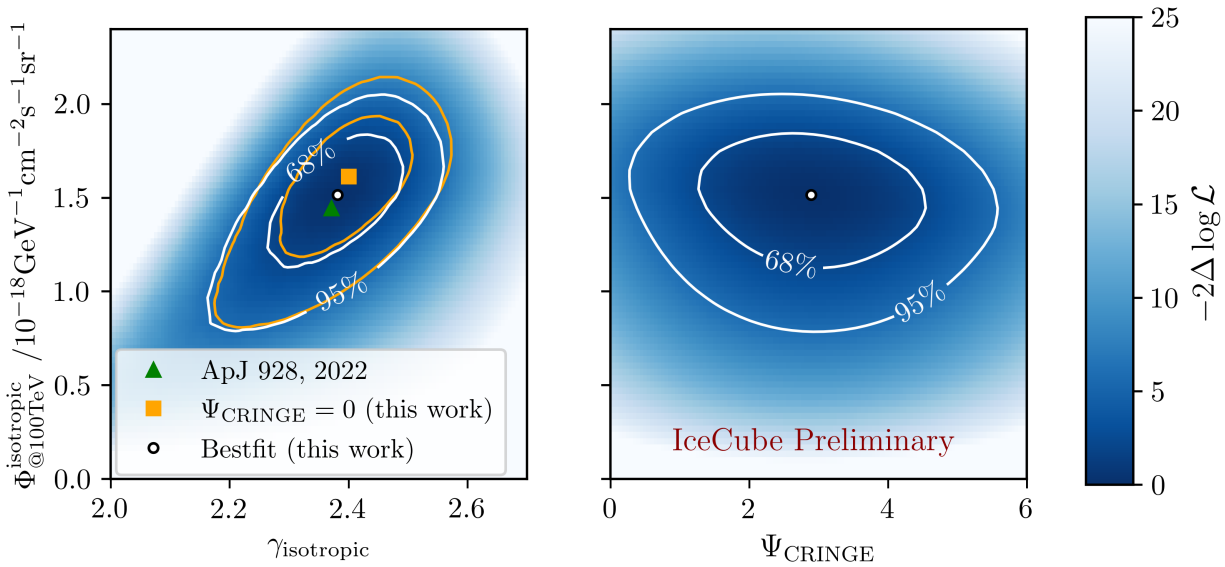

Figure 7.1: Best-fit parameter in a profile likelihood landscape for the galactic plane analysis from Philipp Fürst. In the left plot, the likelihood landscape is shown depending on the diffuse flux normalization and the spectral index. The best-fit parameters for Philipp Fürst's analysis are marked, including the confidence contour, with (white) and without (orange) considering CRINGE contribution. The likelihood landscape of CRINGE and diffuse flux normalization is shown in the right plot. The 68% contour contains only $\Phi_{\text{CRINGE}}^{\text{IceCube}} > 0$, indicating a CRINGE flux contribution. The plots are taken from [8].

The normalization parameter and spectral index obtained in this thesis are higher than those found by Philipp Fürst (cf. Figure 7.2 (a)). That means, that the energy spectrum of the diffuse flux determined in this thesis has a softer energy spectrum. Comparing the confidence contours of both analyses in Figure 7.1 and Figure 7.2, the $2\,\sigma$ contour of Philipp Fürst's analysis has mild tension with the $1\,\sigma$ contour of this analysis. So the results are marginally compatible. The deviation can be explained by the different modeling of the atmospheric background. The atmospheric background is the most dominant high-energy neutrino flux and as already discussed in subsubsection 6.3.2, the atmospheric flux model is not precise in the lower energy region and can be only adjusted by the normalization parameter. In the analysis of the IceCube collaboration, a model for the primary cosmic ray flux and different uncertainties in the flux model are additionally considered [8]. By using a more precise model for the atmospheric background the total energy spectrum can be used in the maximum likelihood method. This was not possible within this thesis due to deviations of the best-fit result and the data for the energy regions $E_\nu < 10^{2.8}\,\text{GeV}$.

In Figure 7.2 (a), it is shown that the best-fit value of the maximum likelihood fit with no CRINGE contribution, i.e. $\Phi_{\text{CRINGE}} = 0$, is located within the $1\,\sigma$ contour in the likelihood landscape. The confidence intervals also overlap in most parts.

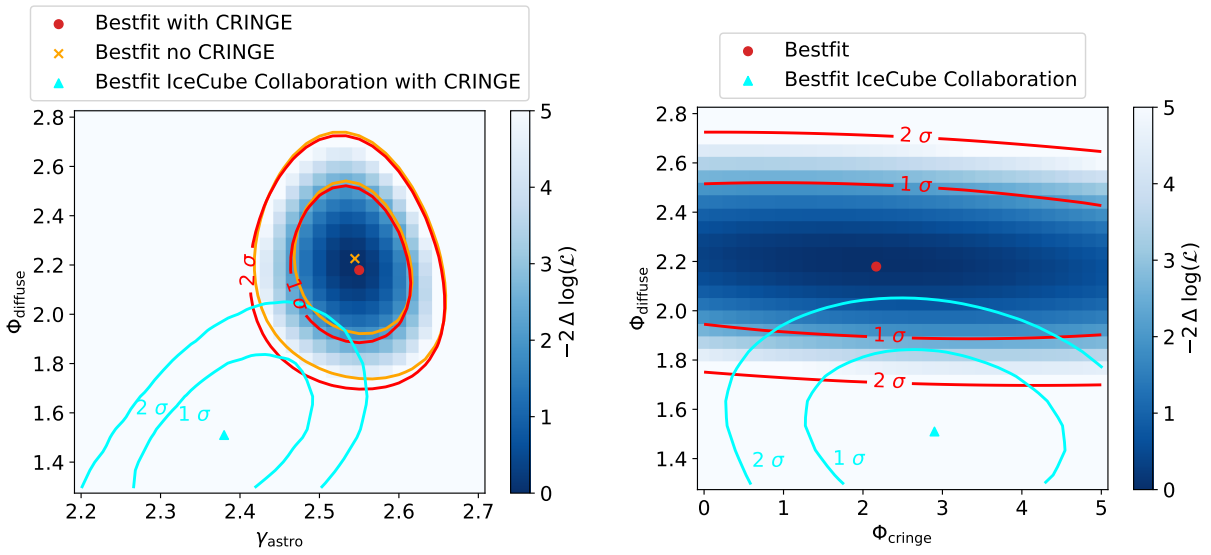

(a) (b)

Figure 7.2: In these plots, a comparison between the best-fit parameters in this thesis and those obtained in Philipipp Fürst's analysis is shown. Figure (a) shows the likelihood landscape including the best-fit values of the diffuse normalization parameter and the spectral index in this thesis, both with and without setting the CRINGE normalization $\Phi_{\text{CRINGE}} = 0$. The best-fit value of the IceCube Collaboration does not fall within the $1\,\sigma$ contour of this thesis. Figure (b) shows the likelihood landscape, including the best-fit values of the diffuse flux normalization and the CRINGE flux normalization. Comparing the best-fit parameter, the best-fit value from the IceCube Collaboration is not contained within the $1\,\sigma$ contour of this thesis.

The minimum in the likelihood landscape of the diffuse astrophysical flux normalization and the CRINGE normalization does not match the best-fit parameter in Philipp Fürst's analysis (cf Figure 7.2 (b)). This is a consequence of the different best-fit values for the diffuse flux normalization. The minima in these profile likelihood plots do only match within the $2\,\sigma$ contours.

8 Conclusion

8.1 Summary

In this thesis, the analysis of the galactic plane is implemented into the PLEnuM framework. Since such an analysis uses a three-dimensional binned maximum likelihood method, the already implemented binned neutrino background model and diffuse astrophysical neutrino model are adapted to a three-dimensional binning. In addition, a model for the galactic neutrino flux, the so-called CRINGE model is implemented.

To test the implementation of the CRINGE model, a model data set is created. Fitting the neutrino flux models to this dataset yields the expected best-fit parameters, as expected. The significance of the rejection of the background hypothesis, i.e. a total neutrino flux without galactic contribution, is determined to be $0.8\,\sigma$ for the model data set. This can be explained by the small contribution of the number of neutrino events in the CRINGE model compared to the total model data set. Based on this result, no higher significance is expected for a real detector data set.

For further testing of the analysis, the analysis is performed on public IceCube data of 6 years. The maximum likelihood method is used to obtain the free model parameters. In this thesis, the best-fit parameters of the model parameters are determined to $\Phi_{\text{background}}^{\text{best-fit}} = 1.30$, $\Phi_{\text{diffuse}}^{\text{best-fit}} = 2.20$, $\gamma_{\text{astro}}^{\text{best-fit}} = 2.54$ and $\Phi_{\text{cringe}}^{\text{best-fit}} = 2.14$. The uncertainties of the fit parameters are obtained by the profile likelihood scans described in subsubsection 6.3.4. A hypothesis test is performed to determine the probability of the background hypothesis, i.e. that there is no galactic contribution in the neutrino flux detected by IceCube. This probability, the p-value, is determined to $p = 0.56$, which is consistent with the analysis on the modeled dataset. Therefore the background hypothesis is accepted and there is no significance for a galactic neutrino flux contribution within this analysis.

In contrast to the analysis presented, Philip Fürst fitted a galactic neutrino contribution with a significance of $2.7\,\sigma$. However, also a different IceCube dataset is used, containing 12.3 years of data, including $982,279$ neutrino events. Within this thesis, a 6-year public dataset is used. Only neutrino events with an energy $E_\nu < 10^{2.8}\,\text{GeV}$ can be fitted, resulting in an energy cut. After the energy cut $403,014$ neutrino events remain. In both analyses, the CRINGE model and a power law for the diffuse astrophysical flux are used. The difference is the modeling of the atmospheric background which is the most dominant high-energy neutrino flux. That is why the best-fit values in the likelihood landscapes plotted in subsection 7.2 are only mildly compatible. Furthermore, the higher significance of Philipp Fürst's analysis results also from the dataset of 12.3 years taken, containing more neutrino events.

8.2 Outlook

In the PLEnuM analysis, a dataset covering the full timescale of the data release also could be implemented, to improve statistical significance. For an improved fitting, it is furthermore advisable to add more free parameters in the atmospheric background model. With that, the atmospheric background model can be adjusted to the data.

The galactic plane analysis in this thesis uses only northern neutrino tracks, which do not cover the galactic center. By including additional neutrinos from the southern sky, the galactic plane would become a more prominent feature in the total neutrino flux. In PLEnuM data from other neutrino telescopes can be implemented to enable resolving the full galactic plane.

Additionally, an analysis of the galactic neutrino flux with PLEnuM can be useful when planning new neutrino telescopes. Within this planning process, simulated datasets can be implemented into the PLEnuM framework. That allows to predict the discovery potential for yet-to-be-built neutrino telescopes.

References

[1] R. Abbasi et al. "Improved Characterization of the Astrophysical Muon–neutrino Flux with 9.5 Years of IceCube Data". In: *ApJ 928 50* (2022). URL: https://iopscience.iop.org/article/10.3847/1538-4357/ac4d29/pdf.

[2] Gisela Anton. "Neutrino Telescopes". In: *Probing Particle Physics with Neutrino Telescopes*. WORLD SCIENTIFIC, Jan. 2020. DOI: 10.1142/9789813275027_0002. URL: http://dx.doi.org/10.1142/9789813275027_0002.

[3] Gerhard Bohm and Günter Zech. "Introduction to Statistics and Data Analysis for Physicists". In: (Jan. 2010).

[4] Ice Cube Collaboration. *IceCube*. URL: https://icecube.wisc.edu/science/icecube/.

[5] IceCube Collaboration. "Observation of high-energy neutrinos from the Galactic plane". In: *Science* 380.6652 (June 2023), pp. 1338–1343. ISSN: 1095-9203. DOI: 10.1126/science.adc9818. URL: http://dx.doi.org/10.1126/science.adc9818.

[6] PD Dr. Thomas Eberl. *Lecture notes in Neutrino Astronomy*. SS 2023.

[7] Gary J. Feldman and Robert D. Cousins. "Unified approach to the classical statistical analysis of small signals". In: *Physical Review D* 57.7 (Apr. 1998). ISSN: 1089-4918. DOI: 10.1103/physrevd.57.3873. URL: http://dx.doi.org/10.1103/PhysRevD.57.3873.

[8] (for the IceCube Collaboration) Fuerst Philipp. "Galactic and Extragalactic Analysis of the Astrophysical Muon Neutrino Flux with 12.3 years of IceCube Track Data". In: *Proceedings of 38th International Cosmic Ray Conference — PoS(ICRC2023)*. ICRC2023. Sissa Medialab, Aug. 2023. DOI: 10.22323/1.444.1046. URL: http://dx.doi.org/10.22323/1.444.1046.

[9] Thomas K. Gaisser, Ralph Engel, and Elisa Resconi. "Neutrino astronomy". In: *Cosmic Rays and Particle Physics*. Cambridge University Press, 2016, pp. 356–373.

[10] IceCube Collaboration. *IceCube Data for Neutrino Point-Source Searches Years 2008-2018*. 2021. DOI: 10.21234/CPKQ-K003. URL: https://arxiv.org/abs/2101.09836.

[11] A. Karle. *IceCube*. 2010. arXiv: 1003.5715 [astro-ph.HE].

[12] Tetiana Kozynets, Anatoli Fedynitch, and D. Jason Koskinen. *Atmospheric Lepton Fluxes via Two-Dimensional Matrix Cascade Equations*. 2023. arXiv: 2306.15263 [astro-ph.HE].

[13] John G. Learned and Karl Mannheim. "High-Energy Neutrino Astrophysics". In: *Annual Review of Nuclear and Particle Science* 50.1 (2000). URL: https://doi.org/10.1146/annurev.nucl.50.1.679.

[14] Lisa Johanna Schumacher. *PLEnuM*. https://github.com/PLEnuM-group/Plenum.

[15] Lisa Johanna Schumacher et al. "PLEνM: A global and distributed monitoring system of high-energy astrophysical neutrinos". In: *Proceedings of 37th International Cosmic Ray Conference — PoS(ICRC2021)*. ICRC2021. Sissa Medialab, July 2021. DOI: 10.22323/1.395.1185. URL: http://dx.doi.org/10.22323/1.395.1185.

[16] Georg Schwefer, Philipp Mertsch, and Christopher Wiebusch. "Diffuse Emission of Galactic High-energy Neutrinos from a Global Fit of Cosmic Rays". In: *The Astrophysical Journal* 949 (May 2023). ISSN: 1538-4357. URL: http://dx.doi.org/10.3847/1538-4357/acc1e2.

[17] John P. Snyder. “Map projections: A working manual”. In: (1987). URL: https://pubs.usgs.gov/publication/pp1395.

[18] Jöran Benjamin Stettner. *PhD Thesis: "Measurement of the Energy Spectrum of Astrophysical Muon-Neutrinos with the IceCube Observatory"*. RWTH Aachen, 2021.

Acknowledgements

Thanks to Claudio and Lisa for supervising me and allowing me to gain insight into the IceCube group and work with PLEnuM. I also want to thank everyone who proofread my thesis and provided me with valuable feedback. And thank you to everyone at ECAP for the warm welcome and enjoyable (and long) coffee breaks.

Erklärung

Hiermit bestätige ich, dass ich die vorliegende Arbeit selbst verfasst habe. Weiterhin habe ich nur die angegebenen Quellen und Hilfsmittel verwendet.

Erlangen, 08.04.2024 Anke Mosbrugger